Statistical palaeomagnetic field modelling and dynamo numerical simulation

G Bouligand, G A Hulot, G A Khokhlov, G A Glatzmaier

Geophys. J. Int. (2005) **161,** 603–626 doi: 10.1111/j.1365-246X.2005.02613.x

Statistical palaeomagnetic field modelling and dynamo numerical simulation

C. Bouligand,[1] G. Hulot,[1,2] A. Khokhlov[1,3] and G. A. Glatzmaier[4]

[1] *Département de Géomagnétisme et Paléomagnétisme, CNRS UMR 7577, Institut de Physique du Globe de Paris, 4 Place Jussieu,* 75252 *Paris cedex 05, France*

[2] *NASA/GSFC, code 921, Greenbelt, MD* 20771, *USA. E-mail: gh@ipgp.jussieu.fr*

[3] *International Institute of earthquake Prediction Theory and Mathematical Geophysics, 79, b2, Warshavskoe shosse* 117556, *Moscow, Russia*

[4] *University of California, Santa Cruz, CA* 95064, *USA*

Accepted 2005 February 9. Received 2004 December 21; in original form 2004 March 2

SUMMARY

By relying on two numerical dynamo simulations for which such investigations are possible, we test the validity and sensitivity of a statistical palaeomagnetic field modelling approach known as the giant gaussian process (GGP) modelling approach. This approach is currently used to analyse palaeomagnetic data at times of stable polarity and infer some information about the way the main magnetic field (MF) of the Earth has been behaving in the past and has possibly been influenced by core–mantle boundary (CMB) conditions. One simulation has been run with homogeneous CMB conditions, the other with more realistic non-homogeneous symmetry breaking CMB conditions. In both simulations, it is found that, as required by the GGP approach, the field behaves as a short-term memory process. Some severe non-stationarity is however found in the non-homogeneous case, leading to very significant departures of the Gauss coefficients from a Gaussian distribution, in contradiction with the assumptions underlying the GGP approach. A similar but less severe non-stationarity is found in the case of the homogeneous simulation, which happens to display a more Earth-like temporal behaviour than the non-homogeneous case. This suggests that a GGP modelling approach could nevertheless be applied to try and estimate the mean $\boldsymbol{\mu}$ and covariance matrix $\boldsymbol{\gamma}(\tau)$ (first- and second-order statistical moments) of the field produced by the geodynamo. A detailed study of both simulations is carried out to assess the possibility of detecting statistical symmetry breaking properties of the underlying dynamo process by inspection of estimates of $\boldsymbol{\mu}$ and $\boldsymbol{\gamma}(\tau)$. As expected (because of the role of the rotation of the Earth in the dynamo process), those estimates reveal spherical symmetry breaking properties. Equatorial symmetry breaking properties are also detected in both simulations, showing that such symmetry breaking properties can occur spontaneously under homogeneous CMB conditions. By contrast axial symmetry breaking is detected only in the non-homogenous simulation, testifying for the constraints imposed by the CMB conditions. The signature of this axial symmetry breaking is however found to be much weaker than the signature of equatorial symmetry breaking. We note that this could be the reason why only equatorial symmetry breaking properties (in the form of the well-known axial quadrupole term in the time-averaged field) have unambiguously been found so far by analysing the real data. However, this could also be because those analyses have all assumed to simple a form for $\boldsymbol{\gamma}(\tau)$ when attempting to estimate $\boldsymbol{\mu}$. Suggestions are provided to make sure future attempts of GGP modelling with real data are being carried out in a more consistent and perhaps more efficient way.

Key words: dynamo theory, geomagnetism, geostatistics, palaeomagnetism, spherical harmonics, statistical methods.

1 INTRODUCTION

The past decade has seen significant progress in our understanding of the origin and behaviour of the magnetic field (MF) of the Earth. Several fully consistent 3-D fluid dynamo numerical simulations have been run with success, showing that a planet with a convecting metallic core, such as the Earth, could indeed spontaneously produce a MF by fluid dynamo action within its core (Glatzmaier &

Roberts 1995; Kuang & Bloxham 1997; Christensen *et al.* 1998). Surprisingly, even though those simulations have been run in parameter regimes known to still be very remote from that of the Earth, the fields produced happen to display a number of Earth-like features, such as a dipole dominant structure and the occurrence of reversals (for a recent review, see e.g. Dormy *et al.* 2000). Those encouraging results obviously call for both improved numerical simulations and more detailed comparisons of the simulated fields with the real main MF produced in the core of the Earth.

Such comparisons are relatively straightforward to carry over the historical period, for which spherical harmonic (SH) models of the MF are available (see e.g. Hulot *et al.* 2002). However, a different approach is required to compare the output of numerical simulations with the numerous, but sparse in time and location, data contained in the palaeomagnetic databases available for recent geological epochs. One approach is particularly well suited, the giant gaussian process (GGP) approach introduced by Constable & Parker (1988). This statistical approach relies on a single formalism that can be used to statistically analyse just as well the historical (Constable & Parker 1988; Hulot & Le Mouël 1994), the archeomagnetic (Hongre *et al.* 1998) and the palaeomagnetic MF (Constable & Parker 1988 and many studies since, see e.g. Kono *et al.* 2000a, Khokhlov *et al.* 2001 and references therein). As we shall see, it also is of straightforward use for analogous analysis of the field produced from numerical simulations.

The GGP approach however relies on a set of assumptions required for the approach to be valid. Observations show that the geomagnetic field experienced many significant changes on timescales of tens to a few thousand years, about a mainly axial dipole field. By contrast, this mean field only very occasionally (on timescales of several hundred thousand years) and suddenly (within a few thousand years) changed its polarity in the past, at times of so-called reversals (see e.g. Merrill *et al.* 1996). Although it would probably be advisable to try and develop a statistical formalism capable of also describing such events, the GGP approach deliberately restricts its scope to studying the field produced by the geodynamo at times of stable polarity, defined as the times when the field fluctuates about a non-zero mean field, with a strong stable axial dipole component. There are at least two reasons for this. One is that we do not yet know enough about reversals to propose a statistical formalism that could also account for them in a fully consistent way. The other is that the GGP approach precisely makes it possible to compare the statistical behaviour of the field before and after reversals. This can usefully shed some light about the exact nature of these events.

Additional simplifying assumptions have otherwise systematically been introduced to ease the data analysis. Those assumptions have been reviewed in a companion paper (Hulot & Bouligand 2005, – this issue, hereafter Paper I,) and shown to often amount to symmetry constraints imposed on the GGP models. However, it is not obvious that the MF of the Earth should satisfy those constraints. In fact and as further noted in Paper I, it would be advisable not to *a priori* enforce any such constraint. *A posteriori* analysis of the symmetries involved in a GGP model accounting for the field could indeed also offer a useful guide to characterize the regime under which the geodynamo has been operating in the past.

In the present paper, we take advantage of numerical simulations from the Glatzmaier & Roberts (1995, 1996, 1997; Glatzmaier *et al.* 1999) dynamo to test the fundamental assumptions underlying the GGP approach, address the symmetry issues raised in Paper I and discuss possible simplifying assumptions. Although quite a few detailed analyses of the field produced by those simulations (Glatzmaier *et al.* 1999; Coe *et al.* 2000; McMillan *et al.* 2001) or by other analogous simulations (Bloxham 2000a,b; Kono *et al.* 2000b; Kono & Roberts 2002; Olson & Christensen 2002; Christensen & Olson 2003) have already been published, only a few (McMillan *et al.* 2001, and to a lesser extent Kono *et al.* 2000b and Kono & Roberts 2002) attempted some tests in connection with the GGP approach. None however, fully addressed the relevance of the GGP approach to characterize the field produced by a (numerical) dynamo. This is the main purpose of the present study.

2 GENERAL BACKGROUND

Let us first briefly introduce the background information we will need (for more details, see Paper I). In a GGP description of a field $\mathbf{B}(\mathbf{r}, t)$ at a time of stable polarity, it is assumed that, at any given time t and location $\mathbf{r}$ outside the core,

$$\mathbf{B}(\mathbf{r}, t) = -\boldsymbol{\nabla} V(\mathbf{r}, t), \tag{1}$$

where:

$$V(\mathbf{r}, t) = a \sum_{n=1}^{\infty} \left(\frac{a}{r}\right)^{n+1} \sum_{m=0}^{n} \left[g_n^m(t) Y_n^{mc}(\theta, \varphi) + h_n^m(t) Y_n^{ms}(\theta, \varphi) \right]; \tag{2}$$

a is an arbitrary reference radius; (r, θ, φ) are the spherical coordinates; $Y_n^{m(c,s)}(\theta, \varphi)$ are the real SH functions of degree n and m, Schmidt normalized; and the $[\, g_n^m(t), h_n^m(t)]$ are the so-called Gauss coefficients that define a vector $\mathbf{x}(t)$, assumed to be a single realization of a multidimensional stationary random Gaussian process, with

$$\text{a statistical mean (or mean model) } E\{\mathbf{x}(t)\} = \boldsymbol{\mu}, \tag{3}$$

$$\text{a covariance matrix } E\{[\mathbf{x}(t) - \boldsymbol{\mu}][\mathbf{x}(t') - \boldsymbol{\mu}]^T\} = \boldsymbol{\gamma}(t' - t), \tag{4}$$

where $E\{\}$ is the statistical expectation, $\boldsymbol{\mu}$ is a vector of components $[\mu(g_n^m), \mu(h_n^m)]$ and $\boldsymbol{\gamma}(t' - t)$ is a matrix of elements $\gamma(x_n^m, x_{n'}^{\prime m'}, t' - t)$, with x and x' being either g or h.

In addition, it is assumed that the covariance matrix $\boldsymbol{\gamma}(\tau)$ decreases fast enough towards zero when τ becomes large (i.e. that the process is short-term memory), to ensure that the process is ergodic for both its mean and its covariance, i.e. to ensure that

$$\lim_{T\to\infty} \bar{\mathbf{x}}_T = \boldsymbol{\mu} \quad \text{and} \quad \lim_{T\to\infty} \bar{\mathbf{K}}_T(\tau) = \boldsymbol{\gamma}(\tau),$$

where we have introduced the following time averages:

$$\bar{\mathbf{x}}_T = \frac{1}{T} \int_0^T \mathbf{x}(t)\, dt, \tag{5}$$

$$\bar{\mathbf{K}}_T(\tau) = \frac{1}{T} \int_0^T [\mathbf{x}(t) - \bar{\mathbf{x}}_T][\mathbf{x}(t + \tau) - \bar{\mathbf{x}}_T]^T \, \mathrm{d}t. \tag{6}$$

Necessary and sufficient conditions can then be derived for a GGP to be either spherically, axially (about the rotation axis of the Earth), or equatorially symmetric in a statistical sense (see Paper I for proofs):

Conditions for spherical statistical symmetry

$$\mu\left(g_n^m\right) = \mu\left(h_n^m\right) = 0, \tag{7a}$$

$$\gamma\left(x_n^m, x_{n'}^{\prime m'}, \tau\right) = 0 \text{ if } x_n^m \neq x_{n'}^{\prime m'} \quad \text{and} \quad \gamma\left(x_n^m, x_n^m, \tau\right) = \gamma_n(\tau); \tag{7b}$$

Conditions for axial statistical symmetry

$$\mu\left(g_n^m\right) = \mu\left(h_n^m\right) = 0 \qquad \text{if} \quad m \neq 0, \tag{8a}$$

$$\gamma\left(g_n^m, g_{n'}^m, \tau\right) = \gamma\left(h_n^m, h_{n'}^m, \tau\right) \qquad \text{if} \quad m \neq 0, \tag{8b}$$

$$\gamma\left(g_n^m, h_{n'}^m, \tau\right) = -\gamma\left(h_n^m, g_{n'}^m, \tau\right), \tag{8c}$$

$$\gamma\left(x_n^m, x_{n'}^{'m'}, \tau\right) = 0 \qquad \text{if} \quad m \neq m'; \tag{8d}$$

Conditions for E^S equatorial statistical symmetry

$$\mu\left(g_n^m\right) = \mu\left(h_n^m\right) = 0 \qquad \text{if} \quad n-m \text{ is odd}, \tag{9a}$$

$$\gamma\left(x_n^m, x_{n'}^{'m'}, \tau\right) = 0 \qquad \text{if} \quad n-m \quad \text{and} \quad n'-m' \text{ are of different parities;} \tag{9b}$$

Conditions for E^A equatorial statistical symmetry

$$\mu\left(g_n^m\right) = \mu\left(h_n^m\right) = 0 \qquad \text{if} \quad n-m \text{ is even}, \tag{10a}$$

$$\gamma\left(x_n^m, x_{n'}^{'m'}, \tau\right) = 0 \qquad \text{if} \quad n-m \quad \text{and} \quad n'-m' \text{ are of different parities.} \tag{10b}$$

As shown in Paper I, a GGP process satisfying eq. (7) would be invariant in any change of frame of reference and thus statistically insensitive to any specific frame of reference. One satisfying eq. (8) would be invariant in any rotation of the frame reference about the rotation axis of the Earth and thus insensitive to any specific longitude. One satisfying eq. (9) would be invariant after reflecting in the equatorial plane and changing the field polarity, and one satisfying eq. (10) would be invariant after reflecting in the equatorial plane. Either way, such a GGP would see both hemispheres in a statistically equivalent way. Thus, a field satisfying either eq. (9) or eq. (10) can be defined as being equatorially symmetric. Introducing the terminology often used in palaeomagnetism (Merrill *et al.* 1996) of dipole family ($n-m$ odd) versus quadrupole family ($n-m$ even), this amounts to say that a GGP will have an equatorial symmetry if and only if $\boldsymbol{\mu}$ belongs exclusively to either the dipole or the quadrupole family and $\gamma(\tau)$ does not couple the two families (for more details, see Paper I).

The general question we now wish to address is the extent to which one may assume that a fluid dynamo of the type thought to be responsible for the main MF of the Earth produces a field that, at times of stable polarity: (i) reasonably complies with a GGP behaviour; (ii) displays meaningful and thus useful statistical symmetry properties that we can identify; and (iii) can be described with the help of reasonably simple $\boldsymbol{\mu}$ and $\gamma(\tau)$.

3 CASE STUDY OF A HOMOGENEOUS NUMERICAL SIMULATION

To address those questions, we first consider the so-called homogeneous model g described in some detail in Glatzmaier *et al.* (1999) and Coe *et al.* (2000). This simulation has been generated by the dynamo model of Glatzmaier & Roberts (1997) that solves the nonlinear magnetohydrodynamic (MHD) equations for the 3-D, time-dependent flow, MF and thermodynamic variables in a rotating, convecting, fluid sphere. Its main characteristic, as far as we are concerned here, is that the convection is thermally driven by homogeneous, i.e. spherically symmetric, thermal boundary conditions. This very high level of symmetry is what makes model g an interesting simulation to investigate first.

The simulation directly produced this field in the form of a time varying geomagnetic model $\mathbf{x}(t)$. Thus, estimates based on eqs (5) and (6) can directly be used to carry on tests. In practice however, we are slightly limited by the length of the simulation, and by the fact that values of $\mathbf{x}(t)$ were saved only up to degree and order 21, and only every approximately 47.5 yr. (Gauss coefficients were indeed saved only every 1000 numerical time steps during the simulation. Because each numerical time step was approximately 17 days, this means that we dealt with snapshots of $\mathbf{x}(t)$ every 47.5 yr; see Glatzmaier *et al.* 1999, for more details.) Fortunately, those limitations do not seriously affect our capacity to draw conclusions. Note also that time in the model is scaled consistently with both the rotation period of the Earth (1 day) and the dipole magnetic diffusion time (20 000 yr). However, this model (like all current models of the geodynamo) should not directly be compared to the actual geodynamo, because the viscous diffusion time of the model is much shorter than the magnetic diffusion time of the Earth.

The simulation has been run over approximately 550 000 yr, but the Gauss coefficients were saved only for a little more than the last 350 000 yr. This amounts to approximately 7500 snapshots (which we will refer to as steps for the purpose of the statistical analysis described below, even though each such step actually represents 1000 time steps in the numerical simulation of Glatzmaier *et al.* 1999). The field produced went through two reversals, which have been studied in detail by Glatzmaier *et al.* (1999), Coe *et al.* (2000) and McMillan *et al.* (2001). Here, we mainly focus on the period of stable polarity between the two reversals. All tests described below therefore deal with the field behaviour between step 2030 and 5020, over a period of $T_0 \approx 142\,000$ yr (step 1 corresponding to the initial step of the last 350 000 yr of the run). In what follows and in order to simplify notations, all time averages $\bar{\mathbf{x}}_{T_0}$ and $\bar{\mathbf{K}}_{T_0}(\tau)$ (as defined by eqs 5 and 6 for the entire period $T = T_0$) will be denoted $\bar{\mathbf{x}}$ and $\bar{\mathbf{K}}(\tau)$.

3.1 Short-term memory

Leaving the issue of stationarity for a later section, we first checked that the field produced by model g is indeed compatible with a covariance matrix $\gamma(\tau)$ decreasing fast to zero when τ becomes large. For each Gauss coefficient $x_n^m(t)$, we computed estimates $\bar{K}(x_n^m, x_n^m, \tau)/\bar{K}(x_n^m, x_n^m, 0)$ of the autocovariance function of $x_n^m(t)$ normalized to its value at $\tau = 0$. Fig. 1 shows the result of such a computation for all $x_n^m(t)$ with degree $n = 2$. It indeed reveals that $\bar{K}(x_n^m, x_n^m, \tau)$ always decreases fast towards zero when τ increases. Similar pictures were obtained for all Gauss coefficients.

In fact, it turns out that all estimates $\bar{K}(x_n^m, x_n^m, \tau)$ take a form very similar to the Gaussian shape Hongre *et al.* (1998) had anticipated for $\gamma(x_n^m, x_n^m, \tau)$:

$$\gamma_n(\tau) = \sigma_n^2 \exp\left[-\frac{\tau^2}{2\tau_n^2}\right], \tag{11}$$

except for the fact that the typical correlation times τ_n involved are not only a function of the degree n, but also of the order m. The only parameter they are not sensitive to is the x character (g or h).

To illustrate this point further, for each Gauss coefficient $x_n^m(t)$, we defined and estimated a typical correlation time τ_n^m as the value of τ such that $\bar{K}(x_n^m, x_n^m, \tau)/\bar{K}(x_n^m, x_n^m, 0) = \exp(-1/2)$. Table 1 lists those estimates for the lowest degrees and Fig. 2 gives a visual account of all values. Again, we see that the τ_n^m strongly depend on both n and m, but are very nearly the same for $g_n^m(t)$ and $h_n^m(t)$ [the differences to be seen are of only a fraction of the time between saved snapshots (47.5 yr) and can therefore be attributed to the limited temporal resolution of the data we analyse]. This, we note, is not compatible with eq. (7b) and may therefore be viewed as a temporal manifestation of some spherical symmetry breaking. By

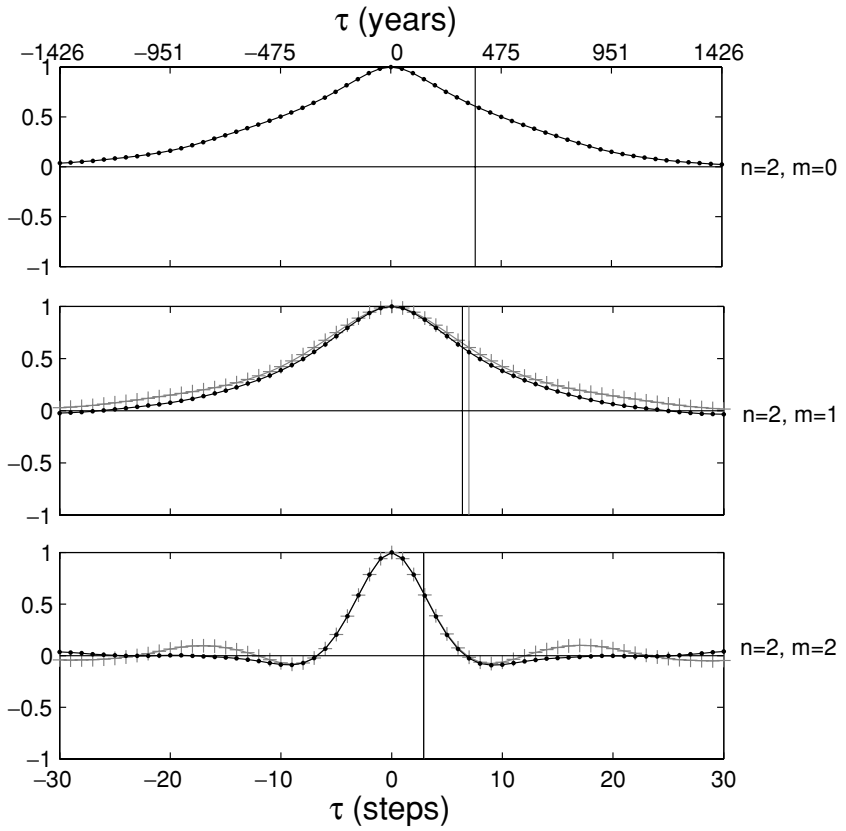

Figure 1. Model g: estimates $\bar{K}(x_n^m, x_n^m, \tau)/\bar{K}(x_n^m, x_n^m, 0)$ of the autocovariance functions normalized to their value at $\tau = 0$, for all Gauss coefficients with degree $n = 2$. The curves with black dots are for the $x = g$ coefficients and those with grey crosses for the $x = h$ coefficients. The time-shift τ is expressed in terms of steps between saved snapshots (lower scale, 1 step = 47.5 yr) and years (upper scale).

Table 1. Model g: estimates of the typical correlation times τ_n^m for the Gauss coefficients with low degrees.

n	m	g steps(yr)	h steps(yr)
1	0	100.4(4772)	
1	1	5.2(249)	4.7(222)
2	0	7.4(354)	
2	1	6.3(297)	6.9(327)
2	2	2.9(137)	2.9(137)
3	0	15.8(752)	
3	1	3.6(171)	3.3(156)
3	2	3.8(179)	3.8(181)
3	3	2.5(117)	2.4(112)
4	0	4.4(210)	
4	1	3.8(181)	3.9(186)
4	2	2.7(129)	2.5(121)
4	3	2.8(132)	2.7(128)
4	4	1.7(82)	1.8(87)

contrast, those results are consistent with the axial symmetry conditions (eq. 8b, with $n = n'$). (Note that timescales cannot bring any information with respect to the third, equatorial, symmetry as eq. 9b/10b involves no requirements on timescales.) Thus, not only is the temporal behaviour of the model g field compatible with a short-term memory process, it also reflects relevant symmetry properties.

3.2 Time-averaged field

We next checked that the field produced by model g is also compatible with a mean field $\boldsymbol{\mu}$ displaying meaningful symmetry properties. We computed time-averaged estimates $\bar{\mathbf{x}}$ of $\boldsymbol{\mu}$ with the help of eq. (5) (Table 2). Of course, none of the $\bar{g}_n^m$ and $\bar{h}_n^m$ we get is exactly zero, because T_0 is not infinite and estimates can only be known to within some statistical bounds. To decide which of those estimates can be considered as significantly different from zero, we relied on the results of Table 1. For each Gauss coefficient $x_n^m(t)$, rather than using the continuous integral (5), we computed an average from samples taken every $\Delta t = 3\tau_n^m$. Those samples may then be considered independent from each other (Hongre *et al.* 1998), which makes it easy to decide whether the resulting average significantly differs from zero or not, with a standard Student's t-test (e.g. van der Waerden 1969; Press *et al.* 1992).

For $g_1^0(t)$, which has the largest $\tau_n^m(\tau_1^0 \approx 4800$ yr, corresponding to approximately 100 time steps), we chose $\Delta t = 302$ steps and an estimate of $\mu(g_1^0)$ was therefore derived from only 10 independent values. The value inferred is nevertheless significantly different from zero at the 10^{-5} per cent level. For all other Gauss coefficients, a Student's t-test at a 1 per cent level was carried out. This leads to the conclusion that estimates of all $\mu(g_n^0)$ significantly differ from zero, except that of $\mu(g_{21}^0)$, which is close to being zero. By contrast, none of the estimates for the 462 non-axial terms appears to significantly differ from zero. This result is consistent with the 1 per cent level of the test over such a population (about four non-zero values being then possibly expected; in fact, the lowest probability we found for a mean non-axial term to be compatible with a zero expected value is of 2.28 per cent, again a reasonable value over such a population). We next reproduced the same test for coefficients up to degree and order 8, more accessible if we were to rely on models derived from observations, at the lower 5 per cent level of significance. Two of

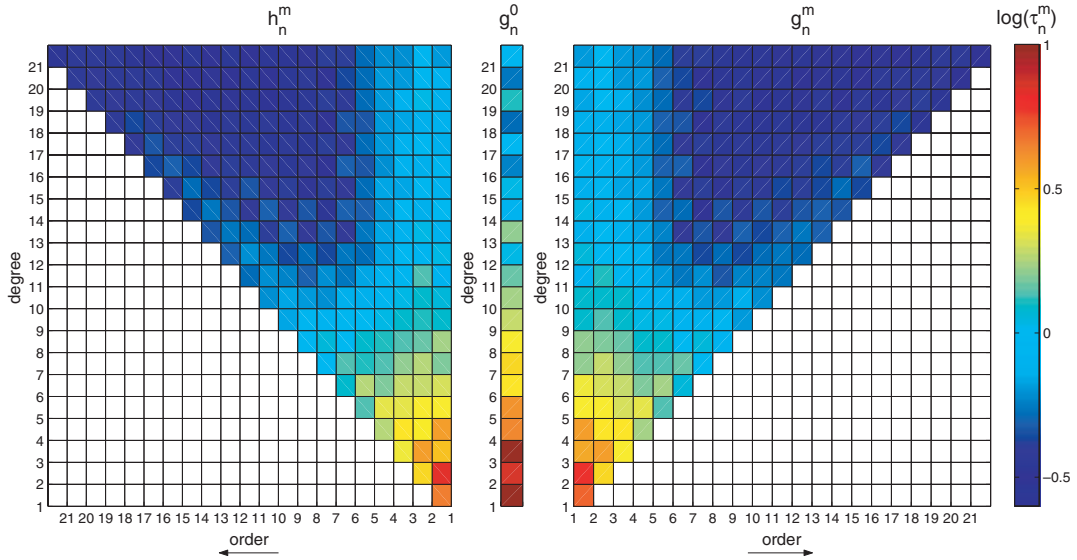

Figure 2. Model g: logarithm representation of the estimates of the typical correlation time $\log_{10}(\tau_n^m)$ for the g and h coefficients, where τ_n^m is scaled with respect to the time between saved snapshots. Hence $\log_{10}(\tau_n^m) = 0$ amounts to $\tau_n^m = 47.5$ yr. Note the central isolated column corresponding to the τ_n^0 only defined for g_n^0 coefficients. Note also the very strong similarity between the τ_n^m for g_n^m and h_n^m when $m \neq 0$.

the 72 estimates for the corresponding non-zonal coefficients were found to be significant (although up to three of those could have been expected; the lowest probability found was then 3.71 per cent).

It thus appears that the time-averaged estimate $\bar{\mathbf{x}}$ of $\boldsymbol{\mu}$ testifies not only for spherical symmetry breaking (eq. 7a is not satisfied) while complying with axial symmetry (eq. 8a is satisfied), but also for some equatorial symmetry breaking. This estimate indeed reveals a mixture of odd (dipole family) and even (quadrupole family) degree zonal fields. Note, however, that it also reveals a mean field quite strongly dominated by the dipole family, especially at the core surface (Table 2).

3.3 Covariances

Consider next the diagonal terms $\gamma(x_n^m, x_n^m, 0)$ of the covariance matrix at time $\tau = 0$ (defining the variances of the x_n^m). Time-averaged estimates $\bar{K}(x_n^m, x_n^m, 0)$ of those can be computed with the help of eqs (5) and (6) (Fig. 3). These estimates are again consistent with some spherical symmetry breaking, as they do not only depend on the degree n, but also on the order m (which conflicts with eq. 7b). They also appear to be consistent with the prediction $\gamma(g_n^m, g_n^m, 0) = \gamma(h_n^m, h_n^m, 0)$ (recall eq. 8b) that axial symmetry be satisfied. Finally, we note that for each degree n, coefficients belonging to the dipole family ($n - m$ odd) again systematically dominate. They clearly display larger variances than those belonging to the quadrupole family ($n - m$ even).

Now, what about cross-covariances? Do estimates of those terms reveal the same symmetry properties? Fig. 4 provides a first answer. It shows estimates $\bar{K}(x_n^m, x_{n'}^{\prime m'}, \tau)/\sqrt{\bar{K}(x_n^m, x_n^m, 0)\bar{K}(x_{n'}^{\prime m'}, x_{n'}^{\prime m'}, 0)}$ of $\gamma(x_n^m, x_{n'}^{\prime m'}, \tau)/\sqrt{\gamma(x_n^m, x_n^m, 0)\gamma(x_{n'}^{\prime m'}, x_{n'}^{\prime m'}, 0)}$, for $x_n^m = g_2^2$ and various values of $x_{n'}^{\prime m'}$ (the normalization by $\sqrt{\gamma(x_n^m, x_n^m, 0)\gamma(x_{n'}^{\prime m'}, x_{n'}^{\prime m'}, 0)}$ being introduced to illustrate the relative importance of the various terms). Those estimates suggest that $\gamma(x_n^m, x_{n'}^{\prime m'}, \tau)$ can be non-zero if $x_n^m \neq x_{n'}^{\prime m'}$, in contradiction with eq. (7b). This again strongly argues in favour of spherical

Table 2. Model g: time-averaged estimates $\bar{g}_n^m$ and $\bar{h}_n^m$ of $\mu(g_n^m)$ and $\mu(h_n^m)$ (at the surface of the Earth and down-continued to the core–mantle boundary, CMB) during the period of reverse polarity.

		At the surface of the Earth		At the CMB	
n	m	g(nT)	h(nT)	g(nT)	h(nT)
1	0	13 700.029 55		83 709.909 32	
1	1	−16.846 94	−7.289 36	−102.938 16	−44.539 41
2	0	−229.104 36		−2559.217 41	
2	1	24.308 93	−18.503 17	271.543 66	−206.690 19
2	2	−17.531 07	17.318 42	−195.831 37	193.455 95
3	0	−372.170 02		−7600.351 31	
3	1	−9.295 33	−6.462 80	−189.826 61	−131.981 42
3	2	−6.698 83	−1.073 79	−136.801 52	−21.928 55
3	3	−2.552 11	15.621 77	−52.118 54	319.023 34
4	0	30.554 19		1140.726 33	
4	1	−0.448 67	9.828 58	−16.750 99	366.945 40
4	2	2.101 79	1.963 82	78.469 37	73.318 18
4	3	−4.766 06	−8.317 76	−177.938 55	−310.539 88
4	4	−1.164 23	4.140 66	−43.466 11	154.589 74
5	0	31.954 74		2181.044 38	
6	0	−3.476 56		−433.807 94	
7	0	3.042 79		694.125 05	
8	0	4.346 78		1812.807 92	
9	0	−2.949 96		−2249.150 45	
10	0	−0.186 80		−260.371 83	
11	0	−0.059 86		−152.540 02	
12	0	0.049 27		229.520 23	
13	0	−0.121 48		−1034.662 02	
14	0	−0.009 26		−144.239 63	
15	0	−0.010 23		−291.290 67	
16	0	−0.000 83		−43.096 80	
17	0	−0.001 91		−181.483 03	
18	0	−0.000 02		−3.152 69	
19	0	−0.000 30		−94.570 20	
20	0	−0.000 01		−4.217 14	
21	0	0.000 00		0.607 55	

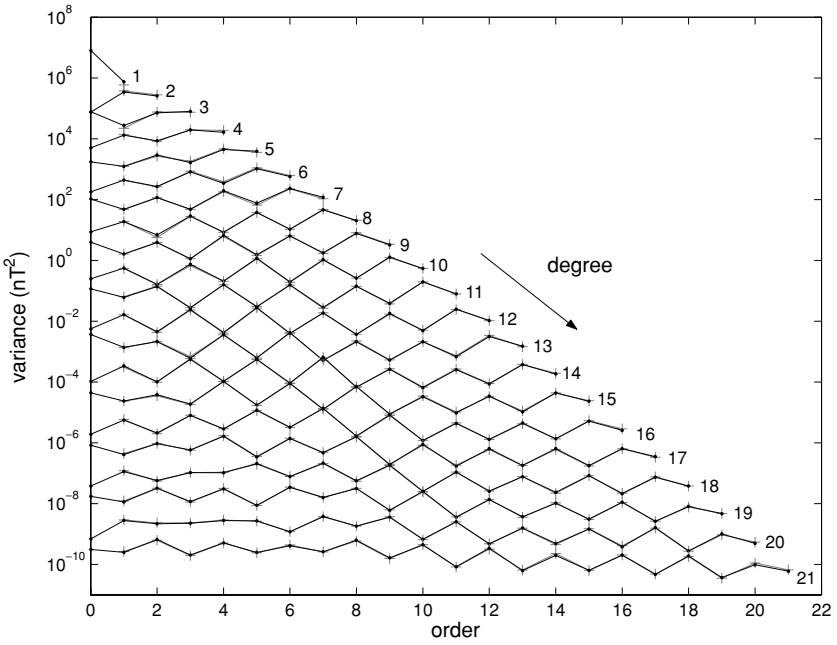

Figure 3. Model g: estimates $\bar{K}(x_n^m, x_n^m, 0)$ of the variances. The black dots represent the values for the $x = g$ coefficients and the grey crosses the values for the $x = h$ coefficients. Coefficients ($x = g$ or h) sharing the same degree are linked for clarity. Note that $\bar{K}(x_n^m, x_n^m, 0)$ is a function of both n and m but not of x. In particular, estimates of variances with $(n - m)$ odd (dipole family) are always larger than those with $(n - m)$ even (quadrupole family).

symmetry breaking. However, those estimates also suggest that this only occurs when $m = m'$ (i.e. for $m = m' = 2$, in the present instance) in agreement with eq. (8d). As a matter of fact, Fig. 4 further suggests that not only eqs (8b) and (8d), but also eq. (8c) (i.e. all axial symmetry requirements) are satisfied. This is tested here for $(n, m) = (2, 2)$, for which estimates suggest that $\gamma(g_2^2, h_2^2, -\tau) = -\gamma(g_2^2, h_2^2, \tau)$ in agreement with the more general constraint:

$$\gamma\left(g_n^m, h_n^m, -\tau\right) = -\gamma\left(g_n^m, h_n^m, \tau\right), \tag{12}$$

equivalent to $\gamma(g_n^m, h_n^m, \tau) = -\gamma(h_n^m, g_n^m, \tau)$ required by eq. (8c). Finally, Fig. 4 would suggest that the equatorial symmetry conditions (9b)/(10b) also are satisfied. Given that eqs (8b–d) are already satisfied, this would indeed only require that $\gamma(x_n^m, x_{n'}^{\prime m}, \tau) = 0$, if n and n' are of different parities, and in particular that $\gamma(g_2^2, g_3^2, \tau) = \gamma(g_2^2, h_3^2, \tau) = 0$, which is what estimates in Fig. 4 indeed suggest is satisfied.

In fact, having visually inspected all cross-covariances in a similar way, we have been led to the conclusion that all estimates were compatible with axial and most equatorial symmetry conditions (8b–d) and (9b)/(10b) but often not compatible with those conditions (7b) not already included in eqs (8b–d) and (9b)/(10b). We could not afford to back this conclusion by systematic statistical tests (to check the level of significance of non-exactly-zero estimates when a zero value was actually expected). However, we did a number of additional calculations for the special case when $\tau = 0$ (i.e. for the estimates $\bar{K}(x_n^m, x_{n'}^{\prime m'}, 0)/\sqrt{\bar{K}(x_n^m, x_n^m, 0)\bar{K}(x_{n'}^{\prime m'}, x_{n'}^{\prime m'}, 0)}$ of $\gamma(x_n^m, x_{n'}^{\prime m'}, 0)/\sqrt{\gamma(x_n^m, x_n^m, 0)\gamma(x_{n'}^{\prime m'}, x_{n'}^{\prime m'}, 0)}$, as $\gamma(x_n^m, x_{n'}^{\prime m'}, 0)$ is the cross-covariance value most relevant in the palaeomagnetic context.

Fig. 5(a) gives a visual account of those estimates, when considering $g_n^m(t)$ and $g_{n'}^{\prime m'}(t)$ up to degree and order $N = 15$. Based on eqs (7) and (8), symmetry breaking of the spherical symmetry without symmetry breaking of axial symmetry should manifest itself by displaying a large number of significant non-zero values among the $m = m'$ estimated cross-covariances, but only a non-significant number of such values among the $m \neq m'$ estimated cross-covariances. This is what Fig. 5(a) suggests. Furthermore, it clearly appears that significant non-zero estimates of $\gamma(x_n^m, x_{n'}^{\prime m}, 0)$ are mainly seen when n and n' are of the same parity (especially when $|n - n'| = 2$). Given that eq. (8) is satisfied, this would again suggest that eq. (9b)/(10b) is almost satisfied and that the fluctuating part of the field indeed tends to also satisfy the equatorial symmetry.

To be more quantitative, we finally relied on a Spearman rank-order correlation test (van der Waerden 1969; Press *et al.* 1992). Testing the significance of the departure of the estimates $\bar{K}(x_n^m, x_{n'}^{\prime m'}, 0)/\sqrt{\bar{K}(x_n^m, x_n^m, 0)\bar{K}(x_{n'}^{\prime m'}, x_{n'}^{\prime m'}, 0)}$ from an expected zero value indeed amounts to test the significance of a possible correlation (or anticorrelation) between the two time-series $x_n^m(t)$ and $x_{n'}^{\prime m'}(t)$ when no time-shift is introduced. This can quantitatively be tested with a Spearman test, provided we sample $x_n^m(t)$ and $x_{n'}^{\prime m'}(t)$ every $\Delta t \geq 3\tau_n^m$ to avoid biases introduced by self-correlation memory issues. We sampled every $\Delta t = 20$ steps (snapshots), which is adequate for all cases, except for $g_1^0(t)$ and $g_3^0(t)$ (recall Table 1). However, this is not a major issue (for those coefficients, separate tests have also been carried out with adequate values of Δt and they led to answers in agreement with those provided here). The results of this Spearman test (also shown on Fig. 5a) confirm most of the previous qualitative results. Among the 119 cross-correlations identified as being significant at the 0.1 per cent level, 103 correspond to cases with $m = m'$ (among which 84 for $m = m' \neq 0$) and only 16 to cases with $m \neq m'$. This leads to a proportion of $103/665 = 15.5$ per cent ($84/560 = 15$ per cent for $m = m' \neq 0$), way above the 0.1 per cent threshold in the $m = m'$ case, which strongly confirms the spherical symmetry breaking. However, it only leads to a proportion of $16/8380 = 0.19$ per cent, very close to the 0.1 per cent threshold, in the $m \neq m'$ case, showing that, by contrast, the axial symmetry is hardly broken.

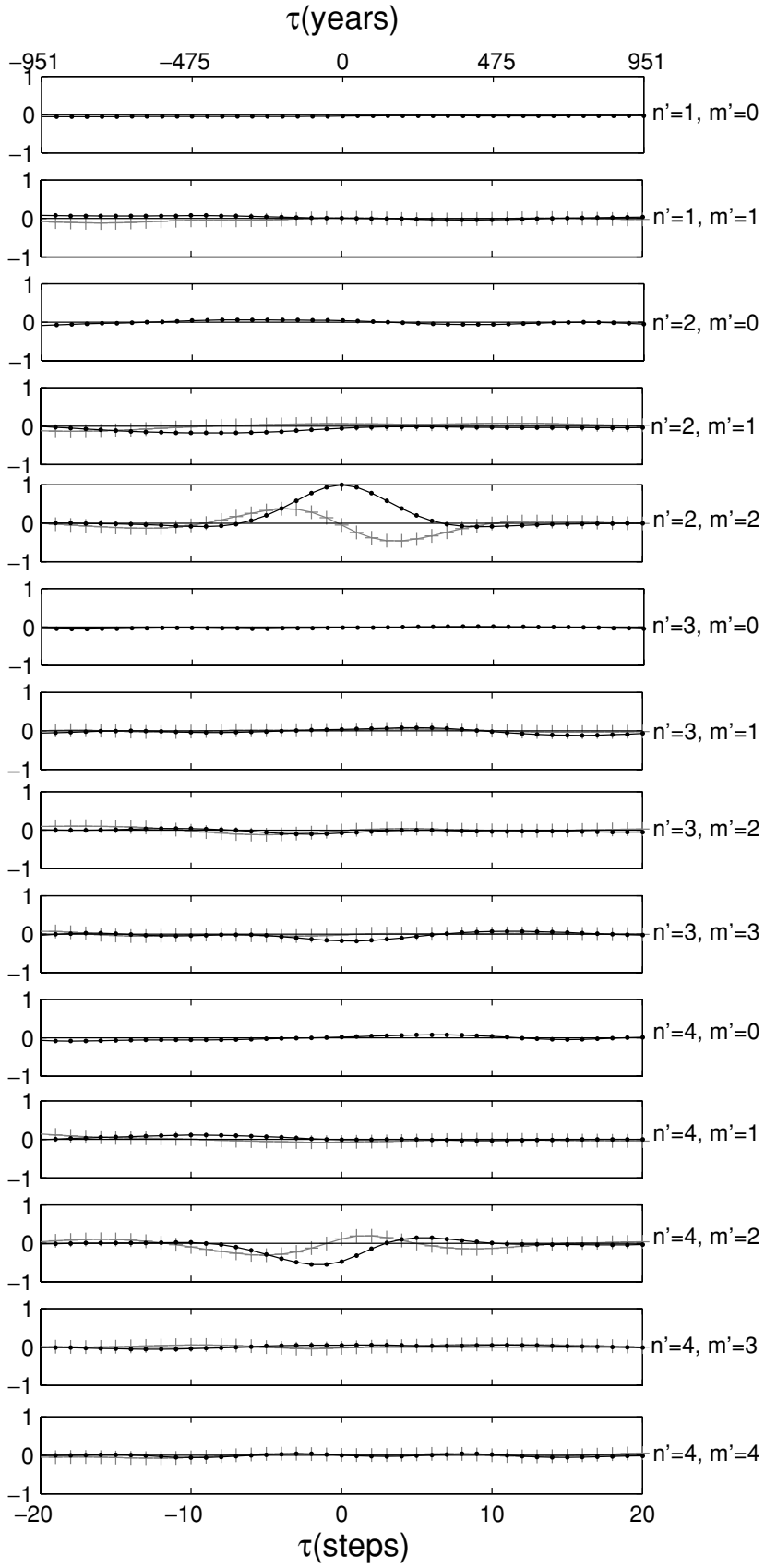

Figure 4. Model g: estimates $\bar{K}(x_n^m, x_{n'}^{\prime m'}, \tau)/\sqrt{\bar{K}(x_n^m, x_n^m, 0)\bar{K}(x_{n'}^{\prime m'}, x_{n'}^{\prime m'}, 0)}$ for $x_n^m = g_2^2$ and all $x_{n'}^{\prime m'}$ with degree $n' \leq 4$. The curves with black dots are for $x' = g$ coefficients and those with grey crosses for $x' = h$ coefficients. The time-shift τ is expressed in terms of steps between saved snapshots (lower scale, 1 step = 47.5 yr) and years (upper scale). Significant values are only found for $n' = 2$, $m' = 2$ and $n' = 4$, $m' = 2$.

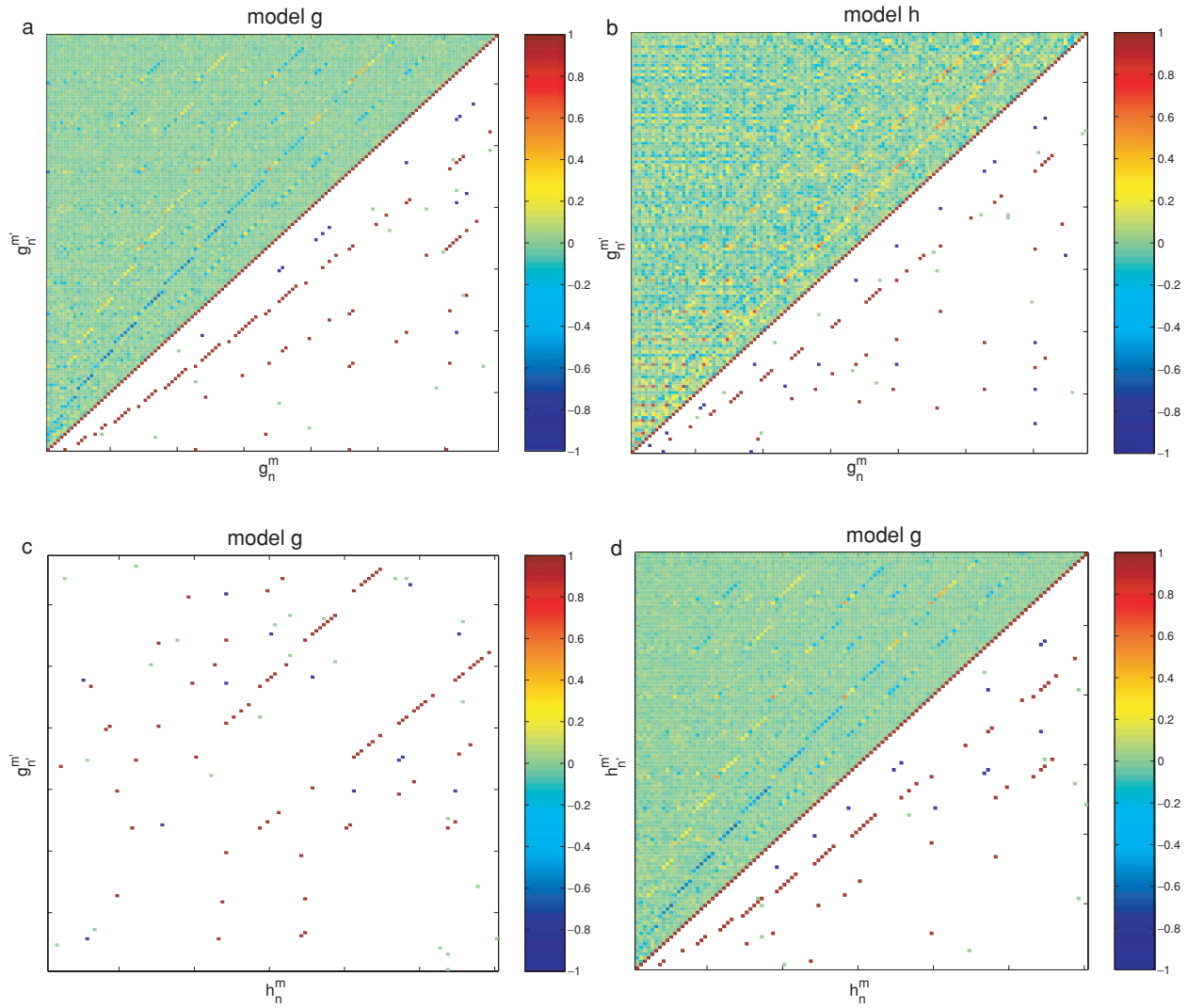

Figure 5. Matrices of the estimates $\bar{K}(x_n^m, x_{n'}^{\prime m'}, 0)/\sqrt{\bar{K}(x_n^m, x_n^m, 0)\bar{K}(x_{n'}^{\prime m'}, x_{n'}^{\prime m'}, 0)}$. Results for model g are presented in (a) when $x = g$, $x' = g$, (c) when $x = h$, $x' = g$ and (d) when $x = h$, $x' = h$. Results for model h when $x = g$, $x' = g$, are otherwise also shown in (b) for comparison with (a). On each axis, the coefficients are ordered with degree and order increasing as follows: $g_1^0\ g_1^1\ g_2^0\ g_2^1\ g_2^2\ g_3^0 \ldots$ and $h_1^1\ h_2^1\ h_2^2\ h_3^1\ h_3^2\ h_3^3 \ldots$ The matrices (a), (b) and (d) being symmetrical by construction, the actual estimates of the cross-correlations are only shown in the upper triangle (see the coloured scale for the value of the estimates) and the result of the Spearman rank-order correlation test on those values at the 0.1 per cent level are shown in the lower triangle. This test is a Student t-test carried on the Spearman rank-order correlation computed with Gauss coefficients sampled every $\Delta t = 20$ steps. For model g, the correlation is thus for instance calculated with 150 points and follows a Student's law with 148 degrees of freedom. A white square means that the correlation is not significant whereas a coloured square means that the correlation is significant, in green when $m \neq m'$, in red when $m = m'$ and $n - n'$ is even, in blue when $m = m'$ and $n - n'$ is odd. For the (c) matrix, which is not intrinsically symmetric, only the results of the Spearman test are shown. Note that for model g significant correlations mainly occur on $m = m'$, $n - n'$ even branches (in red for the Spearman test) and especially on the main branch with $|n - n'| = 2$. Note also the blurring of (b) compared with (a) and the larger number of occurrences of $m = m'$, $n - n'$ odd correlations (in blue for the Spearman test), especially on the $|n - n'| = 1$ branch.

Very similar results are found when considering correlations between $g_n^m(t)$ and $h_{n'}^{m'}(t)$, and between $h_n^m(t)$ and $h_{n'}^{m'}(t)$ (Figs 5c and d). The proportions of significant Spearman cross-correlations then turn out to be of respectively $95/1240 = 7.7$ per cent and $76/560 = 13.6$ per cent, again way above the 0.1 per cent threshold in the $m = m'$ case, and of $24/14\,960 = 0.16$ per cent and $12/6580 = 0.18$ per cent, very close to the 0.1 per cent threshold in the $m \neq m'$ case. In fact, two additional axial symmetry requirements applying to $\gamma(x_n^m, x_{n'}^{\prime m'}, 0)$ when $m = m'$ can then also be checked. First, that $\gamma(g_n^m, g_{n'}^m, 0) = \gamma(h_n^m, h_{n'}^m, 0)$ for $m \neq 0$ (as a consequence of eq. 8b). Very similar values are indeed found for the estimates $\bar{K}(g_n^m, g_{n'}^{m'}, 0)/\sqrt{\bar{K}(g_n^m, g_n^m, 0)\bar{K}(g_{n'}^{m'}, g_{n'}^{m'}, 0)}$ and $\bar{K}(h_n^m, h_{n'}^{m'}, 0)/\sqrt{\bar{K}(h_n^m, h_n^m, 0)\bar{K}(h_{n'}^{m'}, h_{n'}^{m'}, 0)}$ when $m = m' \neq 0$, contrary to the case for $m \neq m'$ (as one would have expected from small quantities differing from zero only because of statistical noise). Secondly, because of eq. (8c), that $\gamma(g_n^m, h_{n'}^m, 0) = -\gamma(h_n^m, g_{n'}^m, 0)$ and $\gamma(g_n^m, h_n^m, 0) = 0$. Those predictions have also been checked.

Finally, the fact that large non-zero estimates $\bar{K}(x_n^m, x_{n'}^{\prime m}, 0)$ are rarely seen when n and n' are of opposite parity can also be quantified. It turns out that approximately 3.0 per cent of all the $|n - n'|$

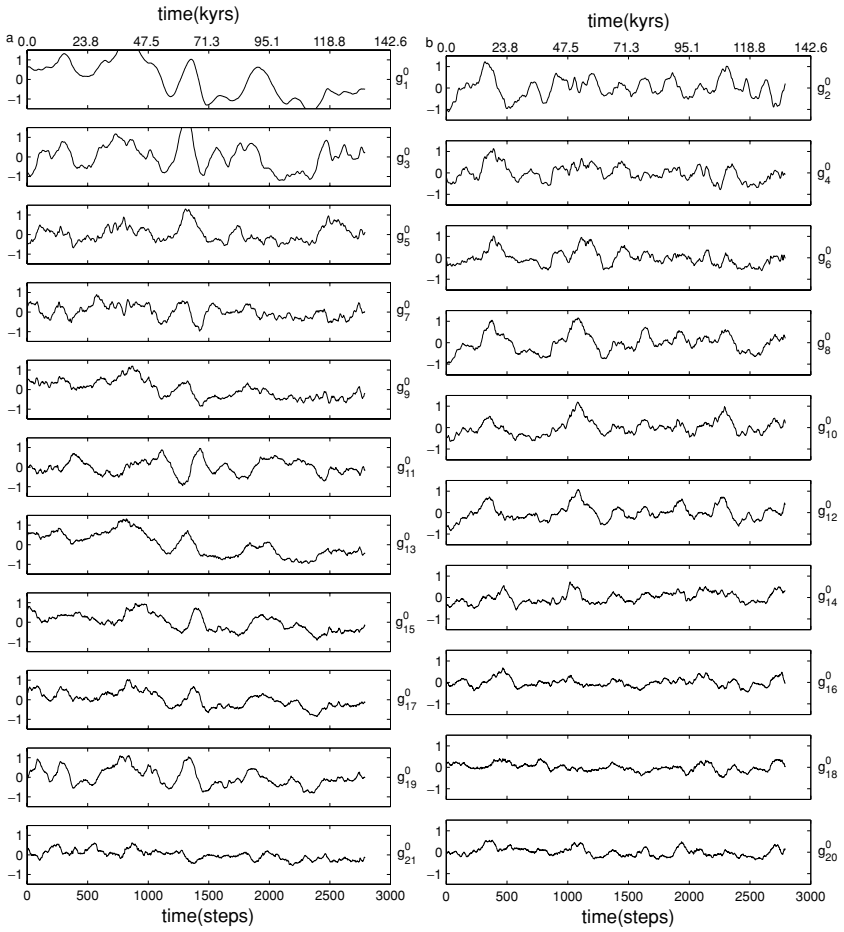

Figure 6. Model g: moving window time averages $\hat{x}_n^m(t)$ (as defined by eq. 13) of the zonal Gauss coefficients [with (a) odd and (b) even degree]. The length of the window is $T_{mw} = 101$ points (4750 yr). The first step of this figure corresponds to a window at the beginning of the period of reverse polarity (i.e. centred about step 2130 in the text).

odd cases up to degree 15 (Figs 5a, c and d) display a significant correlation at the 0.1 per cent level. This interesting result shows that $|n - n'|$ odd correlations are indeed rare, but nevertheless occur more often than possible by sheer chance, testifying for some slight but significant equatorial symmetry breaking.

From all this we conclude that, just as for $\bar{\mathbf{x}}$ with respect to $\boldsymbol{\mu}$, the time-averaged estimate $\bar{\mathbf{K}}(\tau)$ of the covariance matrix $\boldsymbol{\gamma}(\tau)$ clearly testifies for spherical symmetry breaking while complying with axial symmetry requirements. Evidence for equatorial symmetry breaking is also found, but in a much weaker form than for $\boldsymbol{\mu}$. Finally and beyond any symmetry issue, it is important to note that significant non-zero estimates of $\gamma(x_n^m, x_{n'}^{\prime m}, 0)$ are only found when $|n - n'|$ remains small.

3.4 Non-stationarity

Let us now address the stationarity issue. For each Gauss coefficient $x_n^m(t)$, we first computed moving window time averages of the coefficient itself, corrected for the estimated mean $\bar{x}_n^m$ over the whole period and renormalized by its estimated standard deviation $\sqrt{\bar{K}(x_n^m, x_n^m, 0)}$:

$$\hat{x}_n^m(t) = \frac{1}{T_{mw}} \int_{-T_{mw}/2}^{T_{mw}/2} \frac{\left[x_n^m(t+\tau) - \bar{x}_n^m\right]}{\sqrt{\bar{K}\left(x_n^m, x_n^m, 0\right)}}\, \mathrm{d}\tau. \tag{13}$$

In practice, we chose $T_{mw} \approx 4750$ yr (such that the average in eq. 13 is computed over 101 point values).

Were the Gauss coefficients $x_n^m(t)$ to behave as expected, one would expect each $\hat{x}_n^m(t)$ to behave like a time-dependent estimate of the mean of a series produced by a stationary random Gaussian process, with the same memory, a unit variance and a zero mean. We checked and found this to reasonably be the case for the non-zonal coefficients. However, the situation was found to be different for the zonal coefficients $g_n^0(t)$. Fig. 6 clearly shows that, in addition to the expected short-term fluctuations, all $\hat{g}_n^0(t)$ show slower, larger than expected fluctuations. In addition, it appears that all $\hat{g}_n^0(t)$ with n odd (from the dipole family) on one hand and with n even (quadrupole family) on the other hand strongly tend to correlate with each other.

To complement those tests we next computed

$$\hat{\sigma}\left(x_n^m, t\right) = \left\{ \frac{1}{T_{mw}} \int_{-T_{mw}/2}^{T_{mw}/2} \left[\frac{x_n^m(t+\tau) - \bar{x}_n^m}{\sqrt{\bar{K}\left(x_n^m, x_n^m, 0\right)}} - \hat{x}_n^m(t+\tau) \right]^2 \mathrm{d}\tau \right\}^{1/2}, \tag{14}$$

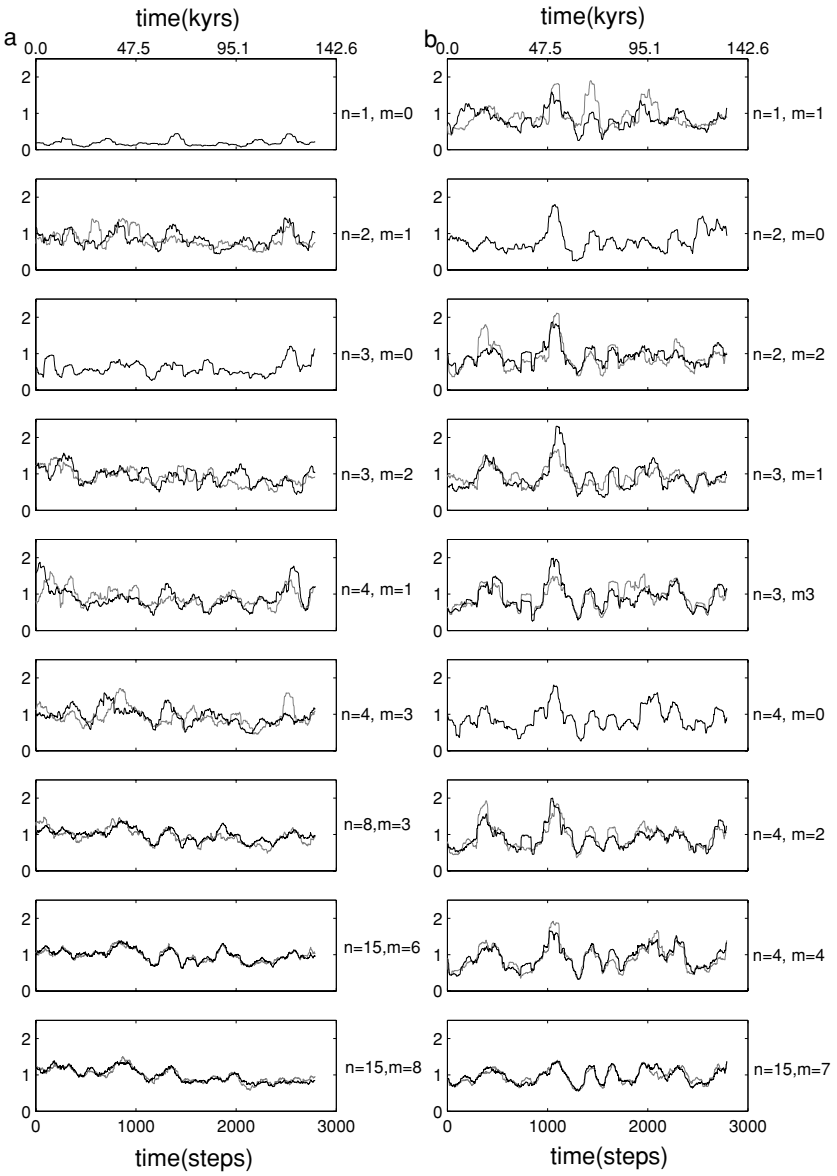

Figure 7. Model g: moving window normalized estimate $\hat{\sigma}(x_n^m, t)$ of the standard deviation (as defined by eq. 14). The black curves are for the g coefficients and the grey curves for the h coefficients. The length of the moving window and the timescale are the same as in Fig. 6.

which may be viewed as a time-dependent normalized estimate of the standard deviation of $x_n^m(t)$ over the same moving window. Fig. 7 shows the $\hat{\sigma}(x_n^m, t)$ computed in this way up to degree and order 4 and for a few additional coefficients with higher degrees. Those again reveal strong long-term fluctuations that, as we tested, cannot be explained within the context of the stationary assumption. In fact, it further turns out that, again within each dipole/quadrupole family, those fluctuations tend to correlate with each other. We checked the extent of these correlations by using a Spearman approach identical to the one we used to investigate cross-covariances and constructed matrices analogous to those shown in Fig. 5. This led to the confirmation of the previous impression. It also led to the conclusion that by contrast virtually no correlations are to be found between $\hat{\sigma}(x_n^m, t)$ with $n - m$ of opposite parity (i.e. not belonging to the same dipole/quadrupole family).

In fact, it further turns out that all the $\hat{\sigma}(x_n^m, t)$ from one family tend to also correlate with the $\hat{g}_n^0(t)$ from the same family. This finally led us to compute stacks $\hat{\sigma}_d(t)$ and $\hat{\sigma}_q(t)$ of the $\hat{\sigma}(x_n^m, t)$ for respectively the dipole ($n - m$ odd) and quadrupole ($n - m$ even) families, and to compare those to the following quantities:

$$G_d(t) = \frac{1}{T_{mw}\bar{g}_1^0} \int_{-T_{mw}/2}^{T_{mw}/2} g_1^0(t+\tau)\,\mathrm{d}\tau$$

and

$$G_q(t) = \sum_{n \text{ even}} \frac{1}{T_{mw}\bar{g}_n^0} \int_{-T_{mw}/2}^{T_{mw}/2} g_n^0(t+\tau)\,\mathrm{d}\tau, \tag{15}$$

which may be viewed as, respectively, the function that slowly modulates the mean dipole family field about its overall average value [$g_1^0(t)$ being the dominant dipole family coefficient], and the function that slowly and independently modulates the mean quadrupole family field (we take a stack because in the quadrupole family no clear coefficient dominates at the core–mantle boundary, CMB).

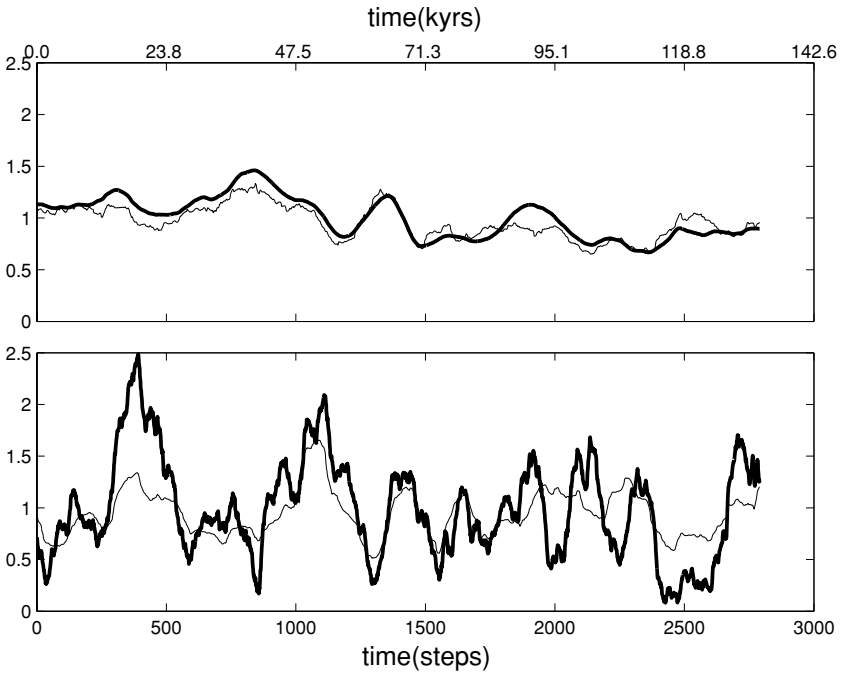

Figure 8. Model g: (upper figure) comparison of $G_d(t)$ (as defined by eq. 15; thick curve) with the stack $\hat{\sigma}_d(t)$ of the $\hat{\sigma}(x_n^m, t)$ with $n - m$ odd (thin curve). (Lower figure) comparison of the stack $G_q(t)$ (as defined by eq. 15; thick curve) with the stack $\hat{\sigma}_q(t)$ of the $\hat{\sigma}(x_n^m, t)$ with $n - m$ even (thin curve). The length of the moving window and the timescales are the same as in Fig. 6.

Fig. 8 shows that $\hat{\sigma}_d(t)$ and $\hat{\sigma}_q(t)$ are very similar to $G_d(t)$ and $G_q(t)$, respectively.

All those results show that, at times of stable polarity, the model g field cannot be viewed as the result of a stationary process. However, it could empirically be viewed as the result of two independent stationary processes modulated by two independent slowly varying functions $F_d(t)$ and $F_q(t)$. One process would describe the dipole family field, with slowly varying mean $F_d(t)\boldsymbol{\mu}_d$ and covariance matrix $F_d(t)\boldsymbol{\gamma}_d(\tau)$. The other would describe the quadrupole family field, with slowly varying mean $F_q(t)\boldsymbol{\mu}_q$ and covariance matrix $F_q(t)\boldsymbol{\gamma}_q(\tau)$. Both $\hat{\sigma}_d(t)$ and $G_d(t)$ would then provide estimates of $F_d(t)$ while both $\hat{\sigma}_q(t)$ and $G_q(t)$ would provide estimates of $F_q(t)$.

3.5 Near-Gaussian behaviour

The non-stationarity of the model g field is the first serious departure we have found so far from the properties required for the GGP approach to be valid. It could turn out to be a major problem. However, we note that the timescale involved in this non-stationarity (of order several hundred steps, i.e. of a couple of tens of thousands of years; Figs 6 and 7) is still relatively short with respect to the duration of the period of stable polarity (142 000 yr). Also, we know that palaeomagnetic samples often cannot be dated to within a couple of tens of thousands of years. In practice, GGP investigations of the properties of the field would thus likely ignore this chronology and simply consider, as a whole, all of the data belonging to a period of stable polarity. In that case, the GGP approach could still possibly prove useful, if the overall distribution of the values taken by each $x_n^m(t)$ over the period of stable polarity could be shown to remain consistent with a Gaussian distribution of mean μ_n^m, and variance $\gamma(x_n^m, x_n^m, 0)$.

This is partly supported by Fig. 9, which shows examples of cumulative distribution functions (CDFs) obtained by picking values every $\Delta t = 3\tau_n^m$ (to ensure independence), removing the estimated mean $\bar{x}_n^m$ and renormalizing by the estimated standard deviation $\sqrt{\bar{K}(x_n^m, x_n^m, 0)}$. Those CDFs are then to be compared with the CDFs of a zero mean unit variance Gaussian distribution, constructed with the same number of samples. Clearly the CDFs do a reasonable job, especially those corresponding to low degrees. However, some deviations are found for high degree coefficients, which tend to display too many large values and not enough small values. To assess whether those departures could be linked to the non-stationary behaviour previously identified, we finally also plotted on Fig. 9 the analogous CDFs for the $x_n^m(t)$ after renormalization by either $\hat{\sigma}_d(t)$ (for the dipole family field) or $\hat{\sigma}_q(t)$ (for the quadrupole family field). An encouraging improvement is indeed found.

4 CASE STUDY OF A NON-HOMOGENEOUS NUMERICAL SIMULATION

Let us now turn to the second simulation of interest, the so-called tomographic model h, also described in some detail in Glatzmaier *et al.* (1999) and Coe *et al.* (2000). Just like model g, this simulation has been generated by the dynamo model of Glatzmaier & Roberts (1997). Both simulations have the same basic characteristics (in particular, they are both thermally driven and share the same dimensional characteristics) except for one minor and one major difference. The minor difference is that the run for model h has only been sampled half as often (every 2000 time steps, so that snapshots, to which we will again refer to as steps in the statistical analysis that follows, are now separated by approximately 95 yr) and not always in a regular way, which forced us to rely on some interpolations. The major difference is of a geophysical nature. Whereas the thermal boundary conditions had been imposed in a uniform way at the CMB in model g, those conditions are now being imposed in a non-uniform way in model h (Fig. 10a). The pattern chosen is one

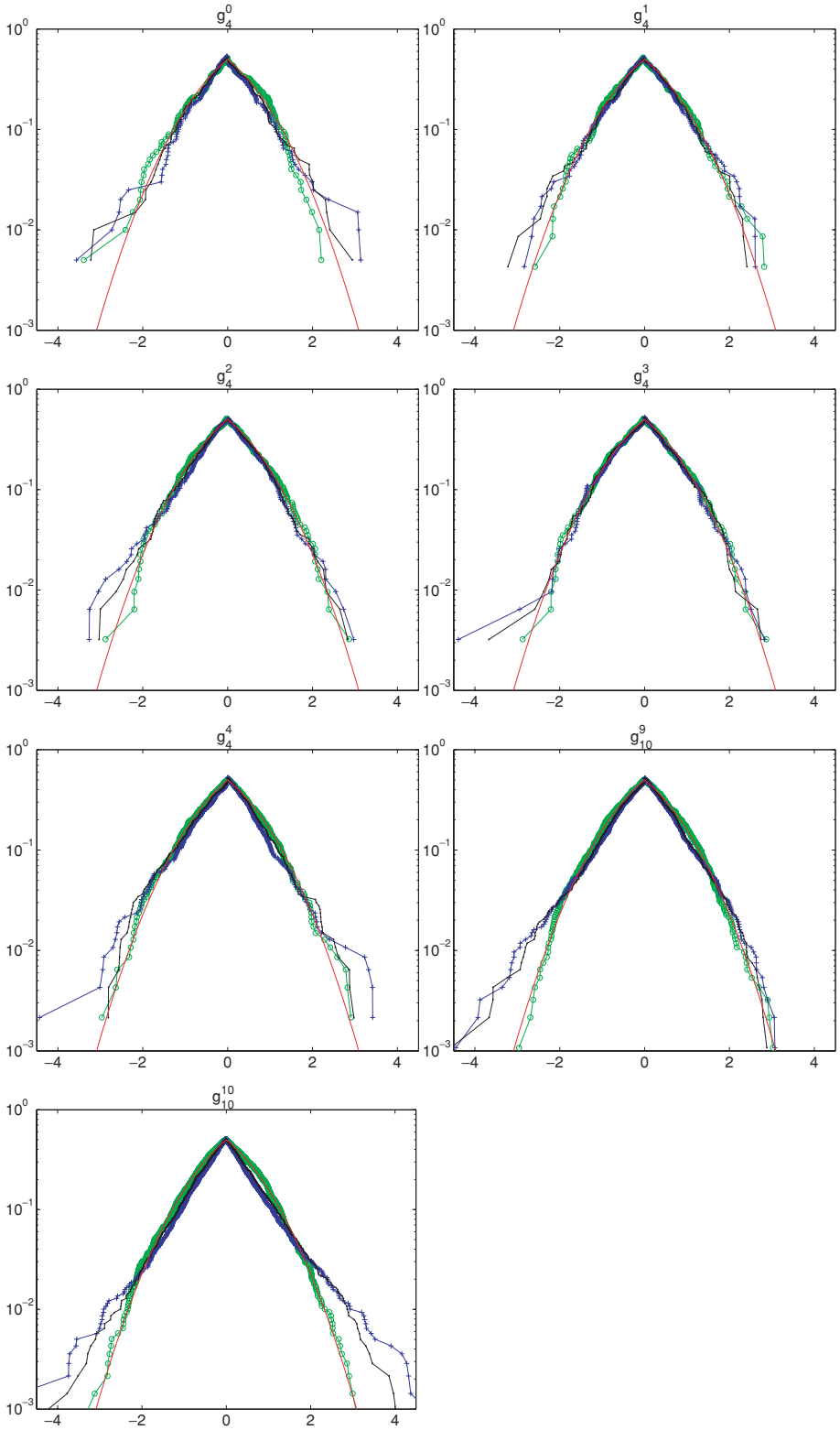

Figure 9. Model g: cumulative distribution functions (CDFs) for a number of Gauss coefficients. A logarithmic scale is used for the vertical scale (y) and the CDF is folded back about the $y = 0.5$ horizontal axis for values above 0.5. This representation makes it possible to better see the behaviour of the distribution away from the (central) most likely values. On each figure, the red curve represents the shape of a theoretical gaussian CDF with zero mean and unit variance. The green curve is a CDF produced from values drawn from such a unit gaussian random distribution, when the number of values is the one involved in the construction of the CDF for the Gauss coefficient of interest, shown in blue [after removal of $\bar{x}_n^m$ and renormalization by $\sqrt{\bar{K}(x_n^m, x_n^m, 0)}$]. Also shown in black, the CDF when the same data are first renormalized by either the stack $\hat{\sigma}_d(t)$ (if the coefficient belongs to the dipole family) or $\hat{\sigma}_q(t)$ (if it belongs to the quadrupole family). Note that the CDF is near, but clearly not exactly Gaussian (here mainly for the g_{10}^{10} coefficient) and that renormalizing by the stacks brings an improvement.

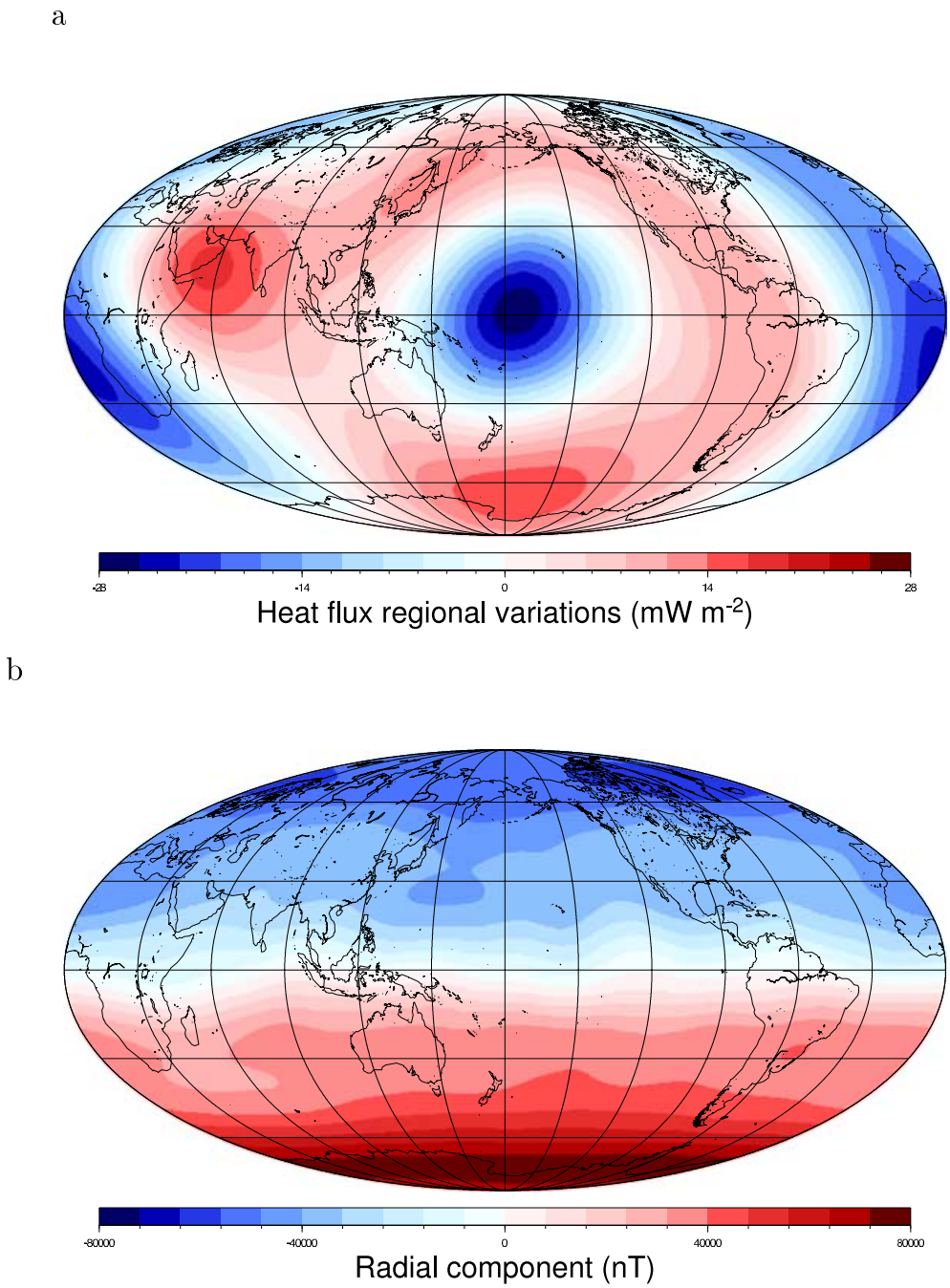

Figure 10. Model h: (a) heat-flux pattern imposed at the core–mantle boundary (CMB; colour scale from -28 to $+28$ mW m^{-2}; for more details, see Coe *et al.* 2000); (b) radial component of the time-averaged field at the CMB calculated during the period of normal polarity (step 1 to 1650) (colour scale from $-80\,000$ to $+80\,000$ nT).

reflecting the modern heat-flux pattern, assuming the geographical variations seen in the seismic tomography for the lowermost mantle of the Earth are mainly a result of thermal effects. In this respect, it may be viewed as a tentatively realistic, heat-flux pattern. Of particular interest is the fact that this pattern strongly breaks the axial symmetry. It also, but to a lesser extent, breaks the equatorial symmetry. It thus forces a complex geometry on the dynamo. As discussed in Paper I, this should lead to some comparable symmetry breaking in the statistical behaviour of the field. What we would therefore like to test is whether the same type of statistical analysis as the one carried out on model g would be capable of detecting this. More generally, we would like to see how much change such more realistic, boundary conditions could introduce in the general statistical behaviour of the field. For that purpose, we basically reproduced all the tests we had done on model g. This was done on the longest period of stable (normal) polarity, between step 1 and step 1650 of the model h run (i.e. over $T_0 \approx 157\,000$ yr, step 1 corresponding to the initial step of the reliable part of the run), which otherwise displayed two reversals (see Glatzmaier *et al.* 1999). This led to the following results.

Table 3. Model h: estimates of the typical correlation times τ_n^m for the Gauss coefficients with low degrees.

n	m	g steps(yr)	h steps(yr)
1	0	43.2(4109)	
1	1	2.0(191)	1.8(174)
2	0	13.3(1264)	
2	1	1.6(156)	1.9(180)
2	2	1.5(138)	1.3(128)
3	0	9.5(899)	
3	1	1.5(147)	1.6(153)
3	2	1.5(142)	1.7(158)
3	3	1.1(103)	1.1(104)
4	0	2.1(202)	
4	1	1.5(146)	1.5(143)
4	2	1.4(128)	1.3(124)
4	3	1.4(129)	1.2(111)
4	4	0.9(84)	1.0(94)

4.1 Short-term memory

We first produced figures analogous to Fig. 1, which confirmed that the model h field also displayed short-term memories. This then made it possible to again compute typical correlation times. Table 3 lists those values for the lowest degrees and Fig. 11 gives a visual account of all values. Comparing Table 3 with the analogous Table 1 shows that the timescales involved in both models are essentially of the same order of magnitude. The only very significant change is seen in the correlation time of $g_2^0(t)$, which increased from 354 yr (model g) to 1264 yr (model h). Otherwise and as expected, we again see a dependence of the correlation time with both the degree n and order m, testifying for the spherical symmetry breaking.

More of a surprise is the fact that no obvious indication of axial symmetry breaking [different correlation times for $g_n^m(t)$ and $h_n^m(t)$, recall eq. 8] is found for low degrees (Table 3, to be compared to Table 1). In fact, only weak indication can be found in the comparison of Fig. 11(left) with Fig. 11(right), which reveals slightly more differences between the $g_n^m(t)$ and $h_n^m(t)$ than does the comparison of Fig. 2(left) with Fig. 2(right).

4.2 Time-averaged field

We next computed the time-averaged estimate $\bar{\mathbf{x}}$ of $\boldsymbol{\mu}$ with the help of eq. (5) (Table 4). This led to values significantly different from those obtained with model g in many respects. First, we note that estimates $\bar{g}_n^0$ of zonal coefficients are globally weaker. This is true for $\bar{g}_1^0$ (which is more than twice weaker), but also for all other coefficients. Secondly and more importantly, we note that by contrast all non-zonal estimates $\bar{g}_n^m$ and $\bar{h}_n^m$ appear to be much larger, to the extent that some of them now take values almost comparable to the estimate $\bar{g}_n^0$ of the zonal term sharing the same degree. To decide which of all those estimates can be considered as significantly different from zero, we relied on the same procedure as for model g.

For $g_1^0(t)$, which has the largest $\tau_n^m(\tau_1^0 \approx 4100$ yr, corresponding to approximately 43 steps), we chose $\Delta t = 130$ steps and an estimate of $\mu(g_1^0)$ was therefore computed from only 13 independent values. The value inferred is then significantly different from zero at the 10^{-3} level. For all other Gauss coefficients, a Student's t-test at a 1 per cent level was otherwise again carried out. This led to the result that only about half of the estimates of the zonal terms $\mu(g_n^0)$ could actually be considered as significant (those with $n = 1$, 5, 7, 9, 10, 12, 13, 15, 16, 17, 19, 20). By contrast eight of the 462 estimates of the non-axial terms now appear to significantly differ from zero [$\mu(g_2^2)$, $\mu(g_3^2)$, $\mu(h_{11}^2)$, $\mu(h_{11}^5)$, $\mu(g_{14}^5)$, $\mu(g_{15}^5)$, $\mu(g_{16}^5)$ and $\mu(g_{17}^4)$]. This brings two conclusions. First, that the time-averaged estimate $\bar{\mathbf{x}}$ of $\boldsymbol{\mu}$ now shows signs of axial symmetry breaking (though quite marginally so, because four non-zero values could have been expected at the 1 per cent level). Secondly, that this estimate still shows signs of equatorial symmetry breaking, but in a different way than in model g. Co-existence of dipole and quadrupole family fields no longer only occurs in the zonal terms, but is also found in the non-zonal terms, to which the two families contribute more equally.

A similar conclusion is derived from the test at the 5 per cent level up to degree and order 8, which we also reproduced. In addition to

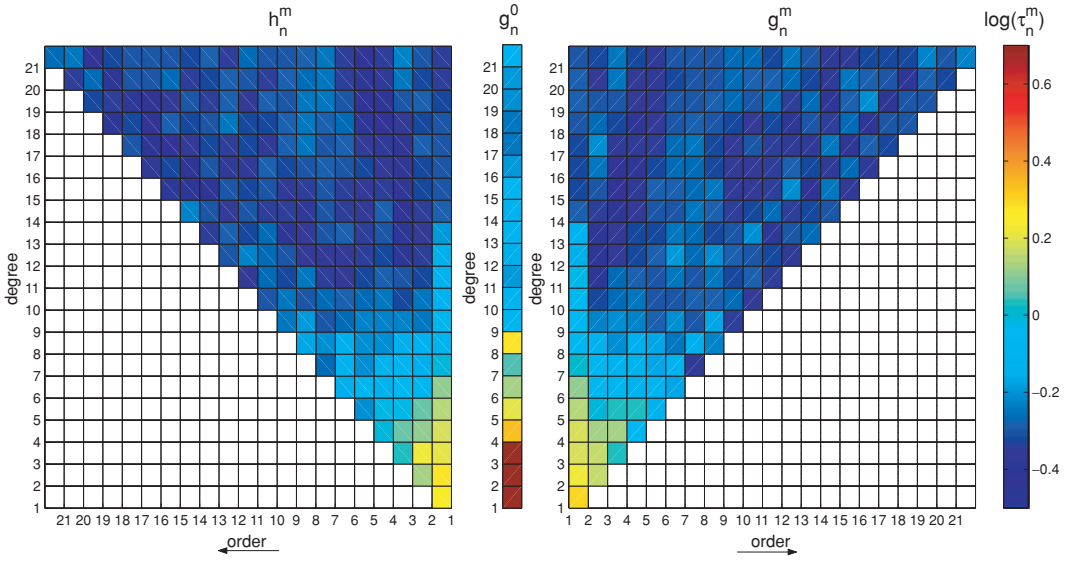

Figure 11. Model h: logarithm representation of the estimates of the typical correlation time $\log_{10}(\tau_n^m)$ for the g and h coefficients. The representation is the same as in Fig. 2 but now the step between saved snapshots is 95 yr. Note the stronger dissimilarities between estimates for the g and h coefficients, compared with model g (Fig. 2).

Table 4. Model h: time-averaged estimates $\bar{g}_n^m$ and $\bar{h}_n^m$ of $\mu(g_n^m)$ and $\mu(h_n^m)$ (at the surface of the Earth and down-continued to the core–mantle boundary, CMB) during the period of normal polarity.

		At the surface of the Earth		At the CMB	
n	m	g(nT)	h(nT)	g(nT)	h(nT)
1	0	−5423.421 58		−33 138.186 12	
1	1	−141.716 70	−90.481 62	−865.917 24	−552.860 70
2	0	242.555 54		2709.474 18	
2	1	32.883 59	49.665 79	367.327 20	554.793 22
2	2	−108.406 89	−48.147 62	−1210.962 55	−537.834 51
3	0	84.295 95		1721.468 23	
3	1	−8.950 96	−3.483 83	−182.793 94	−71.145 72
3	2	−32.690 93	24.635 94	−667.604 98	503.108 28
3	3	−2.933 16	−17.511 01	−59.900 25	−357.604 90
4	0	8.920 05		333.026 07	
4	1	−0.156 86	0.778 95	−5.856 44	29.081 58
4	2	0.704 30	6.038 83	26.294 60	225.456 89
4	3	−3.578 29	0.012 11	−133.593 83	0.452 24
4	4	0.782 88	1.918 17	29.228 60	71.614 03
5	0	−38.601 98		−2634.746 41	
6	0	3.775 55		471.115 60	
7	0	4.839 24		1103.933 34	
8	0	−0.617 04		−257.335 50	
9	0	0.863 91		658.671 94	
10	0	0.047 93		66.814 46	
11	0	−0.021 09		−53.752 87	
12	0	−0.027 48		−128.031 44	
13	0	0.024 71		210.447 50	
14	0	−0.002 43		−37.906 71	
15	0	−0.001 29		−36.824 75	
16	0	−0.000 57		−29.730 00	
17	0	0.000 19		18.212 87	
18	0	−0.000 03		−5.179 65	
19	0	0.000 02		7.758 12	
20	0	0.000 01		3.583 10	
21	0	0.000 00		3.474 54	

$\mu(g_2^2)$ and $\mu(g_3^2)$, estimates revealed two new significant non-zonal coefficients: $\mu(h_3^2)$ and $\mu(h_7^2)$ (four in all, whereas three non-zero values could have been found by chance). This result is again marginal but underlines one additional remarkable property: a dominance of the order 2 in the significant estimates of $\boldsymbol{\mu}$, especially at low degree. Such an order 2 signature is present in the boundary conditions driving model h (Fig. 10a), the pattern of which more generally bears some relation to the pattern of the time-averaged field at the CMB (Fig. 10b).

It thus appears that, as expected, the time-averaged estimate $\bar{\mathbf{x}}$ of $\boldsymbol{\mu}$ not only reveals spherical symmetry breaking, but also some signs of the axial and equatorial symmetry breaking imposed by the CMB conditions. However, it clearly appears that only a careful inspection of the time-averaged field produced by a dynamo driven by inhomogeneous boundary conditions could potentially detect the symmetry breaking introduced by those conditions.

4.3 Covariances

Consider next the estimates $\bar{K}(x_n^m, x_n^m, 0)$ of the diagonal terms $\gamma(x_n^m, x_n^m, 0)$ of the covariance matrix at time $\tau = 0$, computed with the help of eqs (5) and (6) (Fig. 12, to be compared to Fig. 3). Like for model g, those estimates testify for the spherical symmetry breaking, as they do not only depend on the degree n, but also on the order m (which conflicts with eq. 7b). However, they now also provide indications of some axial symmetry breaking, as they now suggest that $\gamma(g_n^m, g_n^m, 0)$ often differs from $\gamma(h_n^m, h_n^m, 0)$ (in disagreement with eq. 8b). Thus, indications for both expected symmetry breakings are found. However, we note that those only occur in a weak way. Also, we note that, contrary to the case of model g, no major difference is to be found between the two dipole and quadrupole families, which now happen to contribute equally to the fluctuating part of the field.

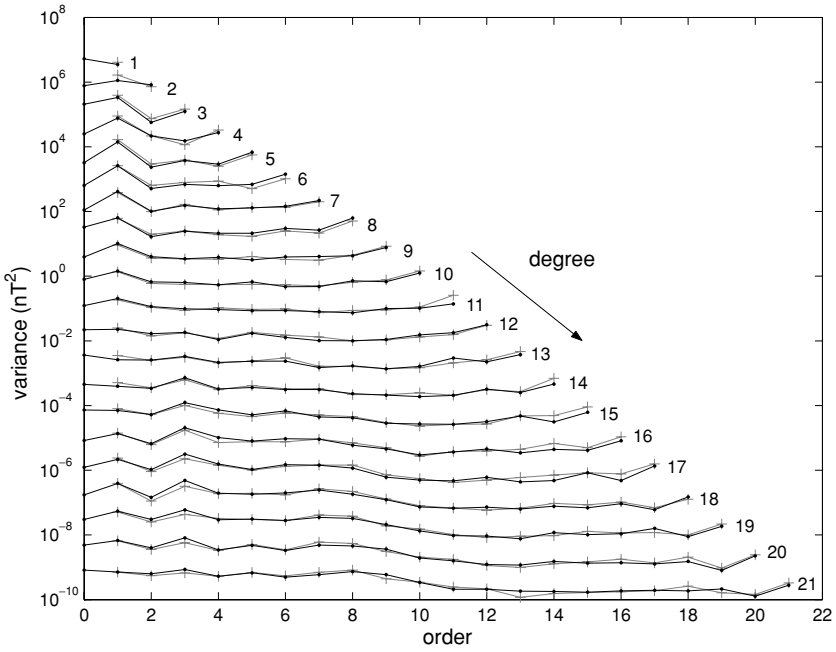

Figure 12. Model h: estimates $\bar{K}(x_n^m, x_n^m, 0)$ of the variances. Same representation as in Fig. 3. Note that compared with Fig. 3 values for g and h no longer overlap and that the dipole family ($n - m$ odd) no longer dominates.

Like for model g, we next computed estimates $\bar{K}(x_n^m, x_{n'}^{'m'}, \tau)/\sqrt{\bar{K}(x_n^m, x_n^m, 0)\bar{K}(x_{n'}^{'m'}, x_{n'}^{'m'}, 0)}$ of the normalized cross-covariance functions for $x_n^m = g_2^2$ and various values of $x_{n'}^{'m'}$ (analogous to those shown in Fig. 4). A clear signature for spherical symmetry breaking could again be seen in the estimate of the cross-covariance functions of g_2^2 with h_2^2 and x_4^2 (just like for model g, not shown). However, again, only weak evidence for additional axial and equatorial symmetry breaking could be found.

In search of additional, perhaps stronger, signatures of axial and equatorial symmetry breaking, we next turned to the systematic analysis of the estimates $\bar{K}(x_n^m, x_{n'}^{'m'}, 0)/\sqrt{\bar{K}(x_n^m, x_n^m, 0)\bar{K}(x_{n'}^{'m'}, x_{n'}^{'m'}, 0)}$ of the normalized cross-covariance functions at time $\tau = 0$. We produced figures analogous to those shown for model g in Fig. 5. Fig. 5(b) shows the result of this when considering $g_n^m(t)$ and $g_{n'}^{m'}(t)$ up to degree and order $N = 15$ (analogous to Fig. 5a). This figure differs from Fig. 5(a) in an interesting way. Whereas nice bands corresponding to $m = m'$ and mainly $|n - n'|$ even $\bar{K}(x_n^m, x_{n'}^{'m'}, 0)$ estimates could clearly be identified against a relatively weak (greenish) background in Fig. 5(a), those bands are now not as easy to identify in Fig. 5(b) and the general background is noisier (colourful). This blurring of Fig. 5(a) into Fig. 5(b) is the type of signature we expected because of the axial symmetry breaking. Also, there clearly is much more of a signal in the $m = m'$, $|n - n'| = 1$, band, suggesting a stronger equatorial symmetry breaking than in model g (contradiction with eq. 9b/10b).

To quantify this, we again relied on the Spearman statistics at the 0.1 per cent level (i.e. counting the number of significant values identified in the bottom right of Fig. 5b). Slightly fewer (93 compared to 119, for model g) cross-correlations are now being identified as significant at this level. Among those, 75 (103 for model g) correspond to cases with $m = m'$ and 18 (compared to 16) to cases with $m \neq m'$. In the $m = m'$ case, this then leads to a proportion of 11.3 per cent (15.5 per cent for model g) way above the 0.1 per cent threshold, which clearly shows that, as expected, model h also strongly breaks the spherical symmetry. For the $m \neq m'$ case, which tests the axial symmetry breaking, the proportion found in model h now only raises to 0.21 per cent (from 0.19 per cent in model g) still very close to the 0.1 per cent threshold. This result is surprising. It would suggest that fluctuations in model h no more strongly break the axial symmetry than in model g, somewhat contradicting the impression given by the comparison of Figs 5(b) and (a). However, there is a reason for this: as axial symmetry breaking can now manifests itself through a very large number of no-longer forbidden coefficients in $\boldsymbol{\gamma}(\tau = 0)$, those become difficult to identify individually in the estimate $\bar{\mathbf{K}}(\tau = 0)$. In particular, the simple statistical tool used here fails to test the full matrix $\bar{\mathbf{K}}(\tau = 0)$ for organized patterns such as those clearly seen in Fig. 5(b). By contrast, equatorial symmetry breaking can more easily be detected. It only requires detecting additional branches in the matrix $\bar{\mathbf{K}}(\tau = 0)$. Indeed, model h displays even more equatorial symmetry breaking than model g. (5.8 per cent of the $m = m'$, $|n - n'|$ odd cases up to degree 15 are found to be significant in Fig. 5(b), compared with 3.6 per cent in Fig. 5(a). As a matter of fact, of all $m = m'$ significant terms we found, 13 per cent were found to be for $|n - n'|$ odd in model g, 28 per cent in model h.) Note finally that independently of any symmetry considerations and as was already the case of model g, significant correlations only occur when $|n - n'|$ remains small.

From those considerations, we conclude that a careful inspection of a time-averaged estimate of the covariance matrix can also potentially detect the symmetry breaking introduced by inhomogeneous boundary conditions driving a dynamo, but not trivially so. In fact, what is best detected is an enhanced amount of coupling between the two dipole/quadrupole family components of the field, testifying for more intense equatorial symmetry breaking in the fluctuating component of the field than in model g. By contrast, detection of axial symmetry breaking, though possible in principle (recall the differences between Figs 5a and b), unfortunately remains elusive.

4.4 Non-stationarity

Like for model g, we next investigated the stationarity of the model h field, by computing $\hat{x}_n^m(t)$ (from eq. 13), and $\hat{\sigma}(x_n^m, t)$ (from eq. 14). Fig. 13 shows that the non-zonal $\hat{x}_n^m(t)$ now display a severe non-stationary behaviour. There clearly are periods when all $\hat{x}_n^m(t)$ take relatively weak values (such as between step 1000 and step 1500 in Fig. 13) and other periods when, by contrast, they all take large values. In particular, the $\hat{x}_n^m(t)$ corresponding to coefficients significantly contributing to the time-averaged field [Fig. 13 displays three of those $\hat{g}_2^2(t)$, $\hat{g}_3^2(t)$ and $\hat{h}_3^2(t)$] appear to contribute to the time-averaged field mainly through relatively short episodes of large values. This contrasts with the behaviour of the zonal terms, those of which contributing to the time-averaged field consistently do so throughout the whole period of interest. This suggests the way model h produces its non-zonal time-averaged field is very different from the way it and also model g produces its zonal time-averaged field. As a matter of fact, all $\hat{g}_n^0(t)$ in model h (Fig. 14) behave in quite the same way as in model g (Fig. 6), except for one significant difference. Whereas in model g the $\hat{g}_n^0(t)$ strongly tend to correlate with each other within the same dipole/quadrupole family, those correlations, though not systematic, now obviously reach across the two families.

Plotting $\hat{\sigma}(x_n^m, t)$ (Fig. 15, analogous to Fig. 7) leads to a similar conclusion. As was already observed for model g, strong correlations are found between the various $\hat{\sigma}(x_n^m, t)$. However, here again, those correlations reach across the two dipole/quadrupole families. In fact, all the $\hat{\sigma}(x_n^m, t)$ obey almost exactly the same very strong modulation. Unfortunately however, this common modulation of all $\hat{\sigma}(x_n^m, t)$ does not appear to be simply related to the way the $\hat{x}_n^m(t)$, especially the non-zonal ones, behave.

We did not attempt to further investigate the nature of this strong and complex non-stationarity, which clearly is in severe contradiction with the GGP assumption.

4.5 Non-Gaussian behaviour

What we did, though, is to finally investigate the extent to which this non-stationarity could also affect the CDFs of the Gauss coefficients. Fig. 16 shows examples of such CDFs for the same Gauss coefficients as those used in Fig. 9 for model g. As can be seen, those CDFs are now dramatically far from being Gaussian. This is again in severe contradiction with the GGP assumption. However, it is important to point out that this is mainly a result of the non-stationary behaviour of model h. To show this, we took advantage of the correlation we already noted among the $\hat{\sigma}(x_n^m, t)$ and produced a stack of those, which we used to renormalize each of the $x_n^m(t)$. The CDFs of those renormalized Gauss coefficients are also shown in Fig. 16. They now display much more of a Gaussian behaviour.

5 DISCUSSION

Having thoroughly investigated the statistical behaviour of models g and h, we can now draw a number of conclusions. Certainly the most

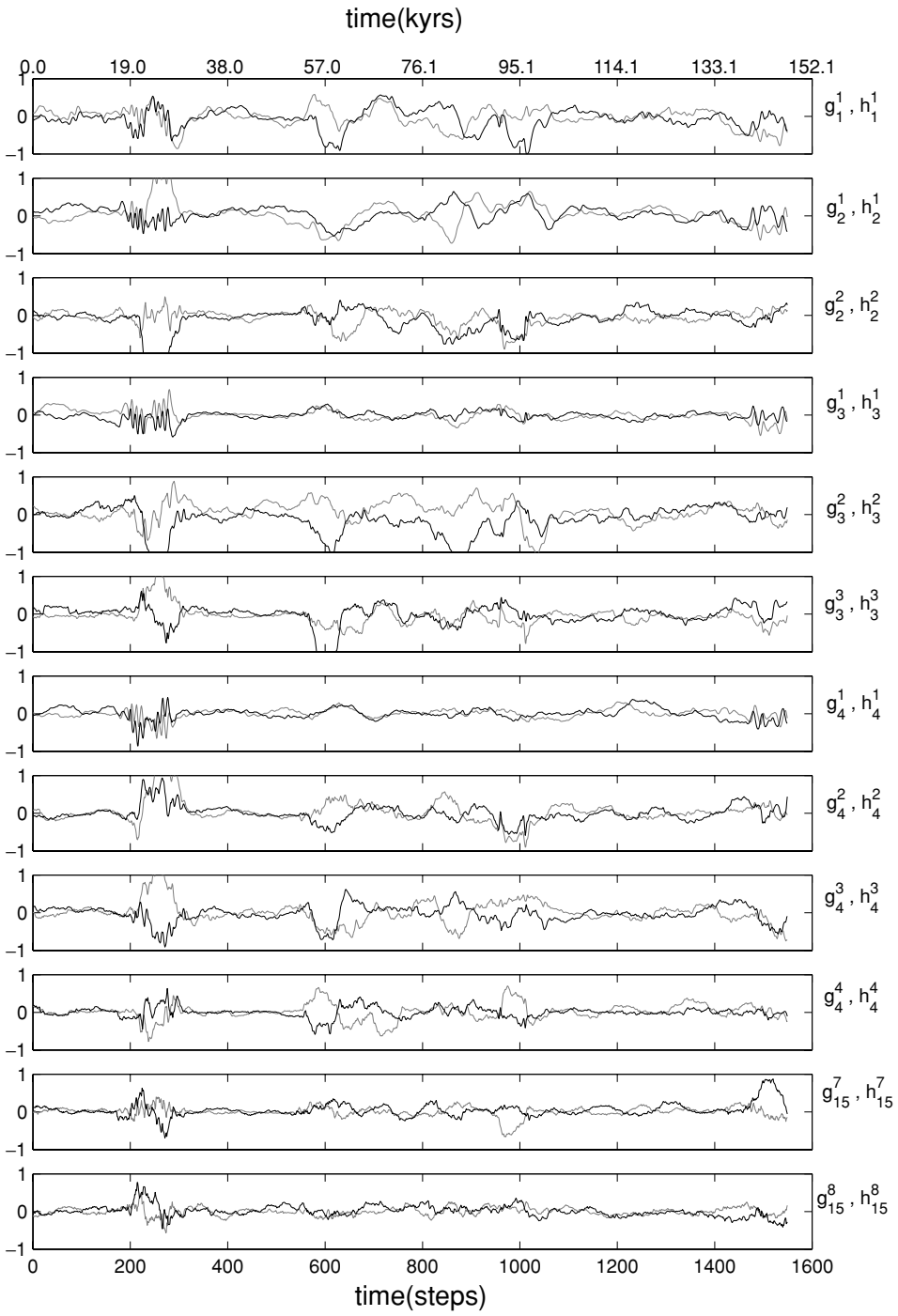

Figure 13. Model h: moving window time averages $\hat{x}_n^m(t)$ (as defined by eq. 13) of non-zonal Gauss coefficients. The length of the window is $T_{mw} = 51$ points (4750 yr). The black curves are for the g coefficients and the grey curves for the h coefficients. The first step of this figure corresponds to a window at the beginning of the period of normal polarity (i.e. centred about step 51 in the text).

important one is the fact that a field produced by a dynamo is indeed amenable to some statistical analysis. The basic assumptions needed for this are satisfied. The field behaves as a short-term memory process at times of stable polarity and periods of stable polarity last much longer than the correlation times of the process. Those properties are needed to define the first- and second-order statistical moments of the field (i.e. the mean $\boldsymbol{\mu}$ eq. 3 and the covariance matrix $\boldsymbol{\gamma}(\tau)$ eq. 4) in a consistent way, and to derive estimates of those from temporal averages (through eq. 5 and eq. 6). This is very encouraging, as it strongly suggests that similar quantities may indeed be defined and estimated for the field produced by the real geodynamo.

A second important conclusion to be drawn is that a careful inspection of estimates of both $\boldsymbol{\mu}$ and $\boldsymbol{\gamma}(\tau)$ can bring some useful geophysical information about the state of the geodynamo, in particular in terms of its symmetry properties. In fact, all symmetry properties one could anticipate on theoretical grounds (Paper I) have been found.

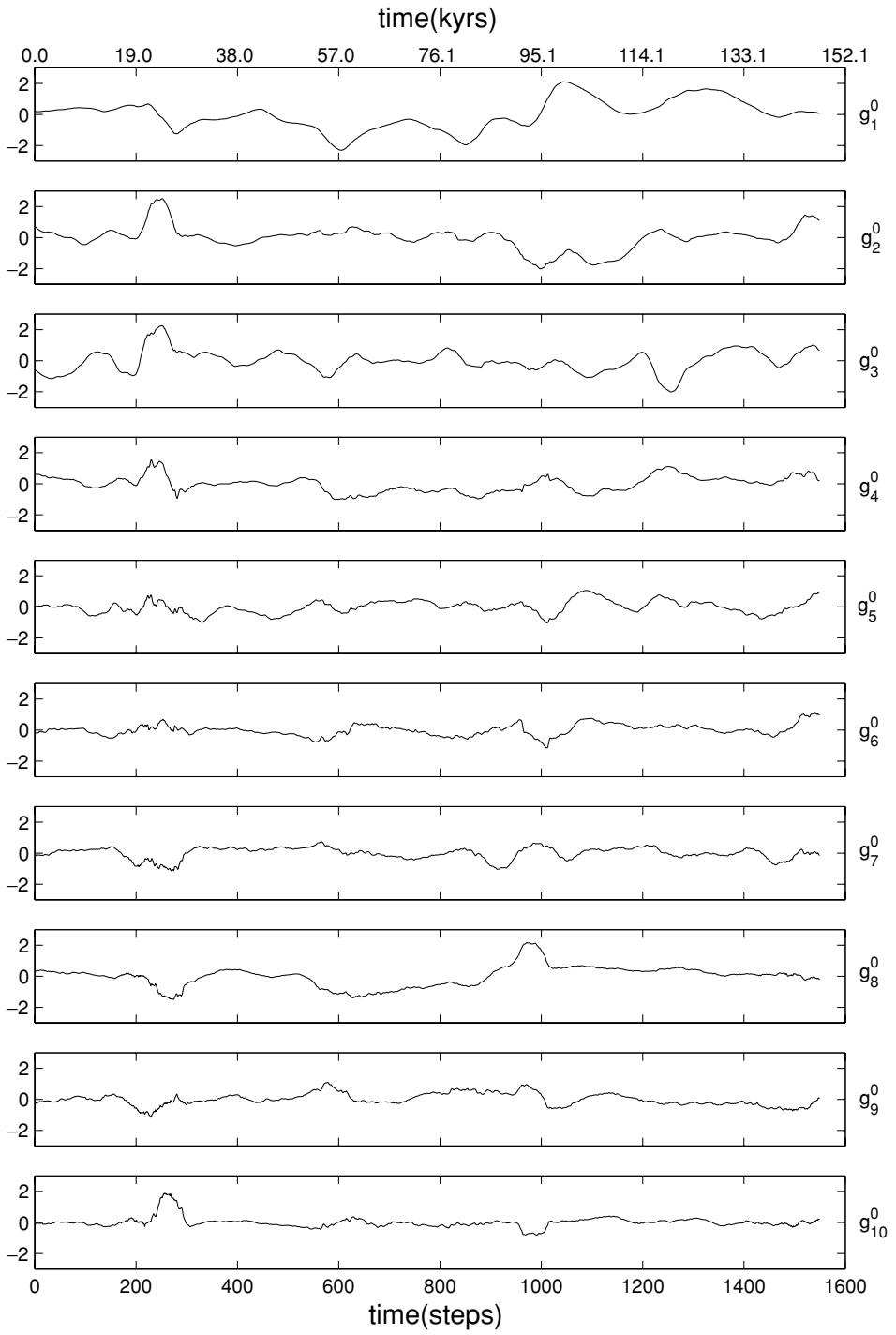

Figure 14. Model h: moving window time averages $\hat{x}_n^m(t)$ (as defined by eq. 13) of the zonal Gauss coefficients. The length of the moving window and the timescales are the same as in Fig. 13.

Consider model g. This model has been run with homogeneous (i.e. spherically symmetric) CMB conditions. However, because of its rotation, the highest symmetry of the whole system is only the axial symmetry about the rotation axis. As noted in Paper I, this means that the field and thus both $\boldsymbol{\mu}$ and $\boldsymbol{\gamma}(\tau)$ should break the spherical symmetry. Additional symmetry breakings could also occur, but only as a result of a spontaneous symmetry breaking by the dynamo solution. They would not be mandatory. In fact, as also noted in Paper I, it is highly unlikely that the axial symmetry could spontaneously be broken because of the ease with which a dynamo solution could shift about the rotation axis under axisymmetric CMB conditions. No similar continuous shift could possibly act against an equatorial symmetry breaking. Thus, it was anticipated that model g would break the spherical symmetry, satisfy the axial symmetry and possibly break the equatorial symmetry. This is what we found. Spherical symmetry breaking is clearly seen in estimates of both $\boldsymbol{\mu}$ and $\boldsymbol{\gamma}(\tau)$; axial symmetry is remarkably satisfied by estimates of both $\boldsymbol{\mu}$ and $\boldsymbol{\gamma}(\tau)$; and evidence for spontaneous equatorial

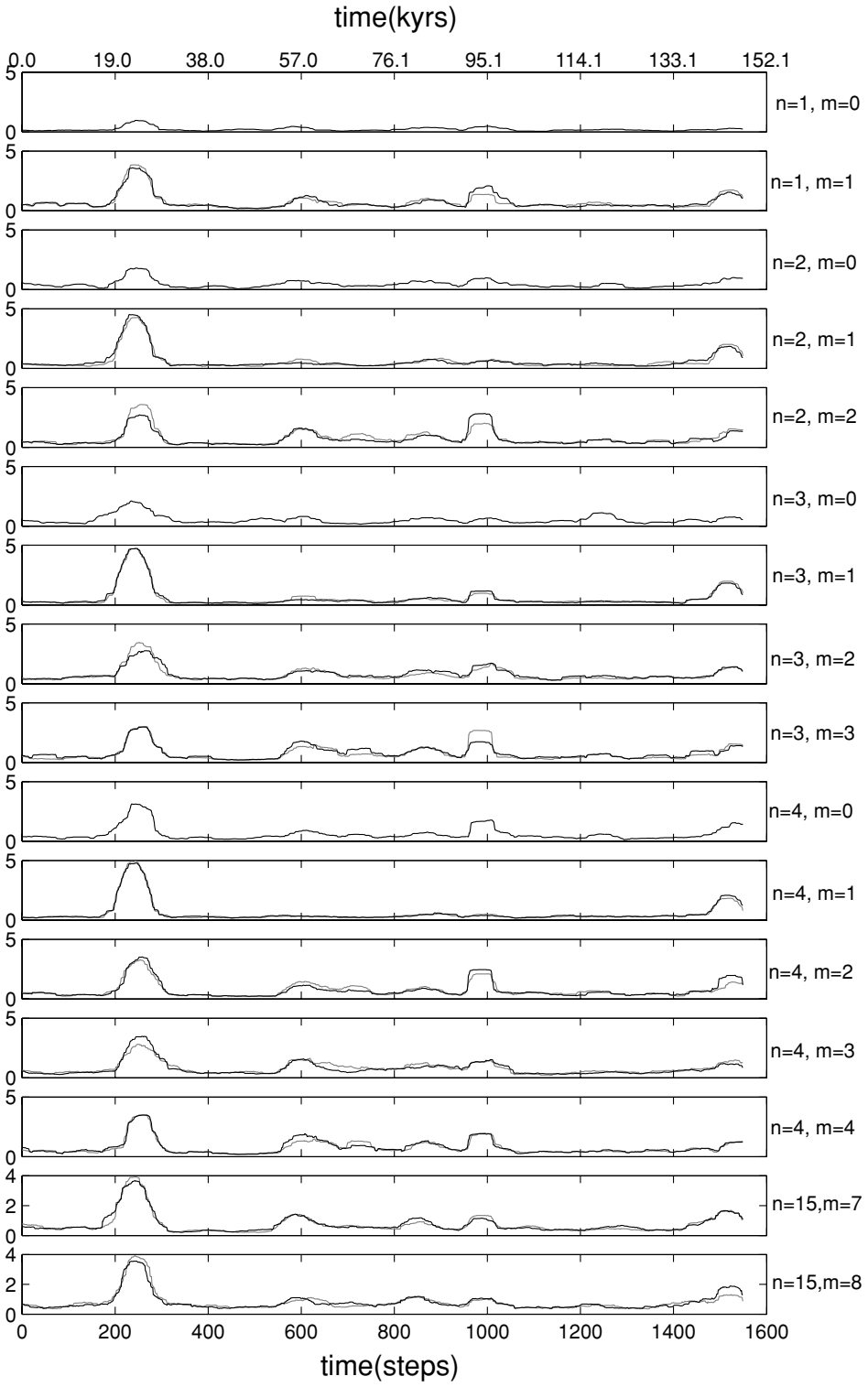

Figure 15. Model h: moving window normalized estimate $\hat{\sigma}(x_n^m, t)$ of the standard deviation (as defined by eq. 14). The black curves are for the g coefficients and the grey curves for the h coefficients. The length of the moving window and the timescales are the same as in Fig. 13.

symmetry breaking was also found in estimates of $\boldsymbol{\mu}$ and (in a subtler way) of $\boldsymbol{\gamma}(\tau)$.

In fact, this spontaneous equatorial symmetry breaking is worth further emphasizing. It is responsible for the co-existence, with the dominant axial dipole mean field, of a quadrupole family zonal mean field and, in particular, of a term $\mu(g_2^0)$ estimated to be approximately 2 per cent the magnitude of the estimate of $\mu(g_1^0)$. From this, we infer that the only unquestionably robust non-dipole feature found so far in the palaeomagnetic mean field, an axial quadrupole field (of about 3–4 per cent the magnitude of the axial dipole field, Merrill & McFadden 2003), cannot alone be taken as evidence of equatorial symmetry breaking in the CMB conditions. In fact and as pointed

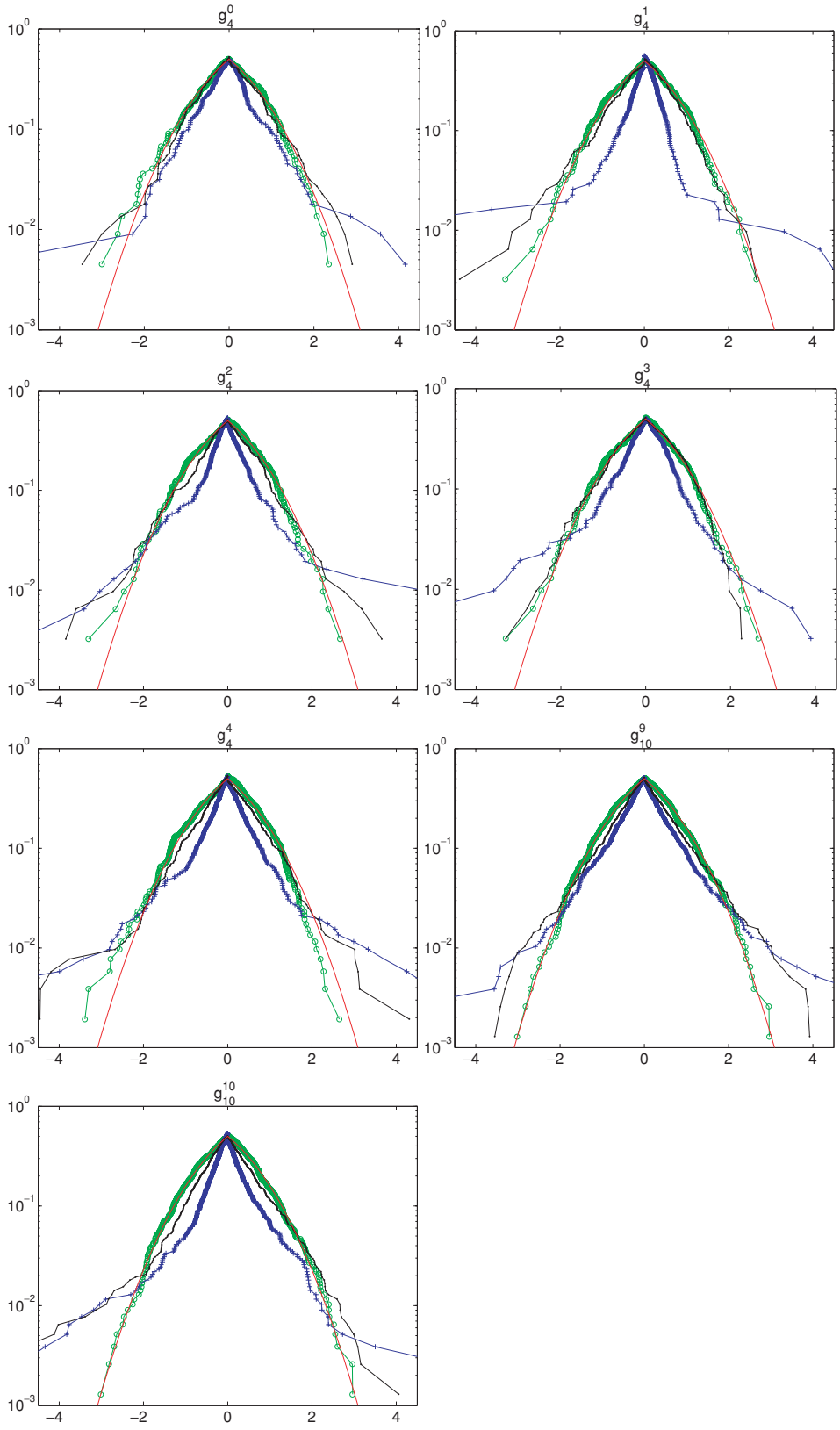

Figure 16. Model h: cumulative distribution functions (CDFs) for a number of Gauss coefficients. Same coefficients and same representation as in Fig. 9, except for the black curves, which now correspond to CDFs after renormalization by a global stack of all the $\hat{\sigma}(x_n^m, t)$. Note the much more serious departure of the CDF from the Gaussian case and the very significant improvement brought by renormalizing by the stack (i.e. correcting for the non-stationarity).

out in Paper I, checking whether this axial quadrupole term could be related to such CMB equatorial symmetry breaking would require further testing if it systematically reverses its sign together with the axial dipole at times of reversals, or not. The test would need to be carried out on both the palaeomagnetic data (palaeomagnetic time-averaged field models would suggest that this is the case, but the case remains to be better made) and the data produced by numerical models with equatorial symmetric CMB conditions, such as model g (the series we currently have are too short to carry out a significant test). If it turns out that the geodynamo can only go through full field reversals [involving a simultaneous sign change of $\mu(g_2^0)$ and $\mu(g_1^0)$], while symmetric CMB conditions dynamo can also go through quadrupole family field reversals [involving a sign change of $\mu(g_2^0)$ but not of $\mu(g_1^0)$] and/or dipole family field reversals [involving a sign change of $\mu(g_1^0)$ but not of $\mu(g_2^0)$], as one can anticipate based on symmetry considerations, then only, a claim could be made that the axial quadrupole component found in the palaeomagnetic mean field is related to some asymmetry in the CMB conditions (see Paper I for more details).

Consider now model h, run with inhomogeneous CMB conditions breaking the spherical, axial and, to a lesser extent, equatorial symmetries. Those conditions were expected to force model h, and thus estimates of both $\boldsymbol{\mu}$ and $\boldsymbol{\gamma}(\tau)$, to testify for similar symmetry breaking properties. Again, this is what we found. In particular, it was found that model h breaks the axial symmetry breaking properties in a way that distinguishes it from model g and testifies for the inhomogeneous CMB conditions imposed on the dynamo.

However, those symmetry breaking properties were only found in the form of weak and subtle signatures in the time-averaged estimates of $\boldsymbol{\mu}$ and $\boldsymbol{\gamma}(\tau)$, some of which turned out to be particularly elusive. Evidencing them required careful statistical assessments. As a matter of fact, earlier analysis of the very same numerical simulation by McMillan *et al.* (2001) failed to identify this signature and reached the opposite conclusion that non-zonal field statistics would not necessarily reflect heat flow conditions at the CMB. In the estimate $\bar{\mathbf{x}}$ of $\boldsymbol{\mu}$ indeed, only a fairly weak non-zonal field could be detected and proven significant. However, this was made possible because correlation times were also derived and taken into account in the statistical assessment. As a result of this, even though most estimates of non-zonal terms turned out to be smaller than zonal terms (Table 4), their shorter correlation times (Table 3) made it possible to prove that at least some of them were meaningful.

Clearly, those results also suggest that if similar significant non-zonal components were to be found in the time-averaged palaeomagnetic field as a result of non-homogeneous CMB conditions, those would likely be weak. Detecting them would again require some careful statistical analysis. In this respect, the fact that the detection of significant non-zonal terms in the actual time-averaged palaeomagnetic field is still a matter of debate (a claim made by e.g. Gubbins & Kelly 1993 and Johnson & Constable 1997, but challenged by e.g. McElhinny *et al.* 1996, Carlut & Courtillot 1998 and Merrill & McFadden 2003) is hardly a surprise. However, those results also show that future investigation of better-constrained time-averaged field models could possibly lead to some inference of the geometrical characteristics of the heat flux at the CMB. This, we should finally point out, would nevertheless require that additional progress in numerical dynamo modelling also be made. First, to better understand the connection between the heat-flux pattern and the pattern of the resulting time-averaged field (beyond the crude connection established in the case of model h). A recent study by Olson & Christensen (2002) suggests this should eventually be possible. Secondly, to make sure that simulations are run with parameters closer to those of the real Earth. An indication that this is needed can be found in the fact that the time-averaged field computed from the recent tomographic model of Christensen & Olson (2003, their fig. 4d), which relies on different parameters than model h but uses similar tomographic boundary conditions, does show substantial differences with that of model h (Fig. 10b).

Another significant outcome of this study is the demonstration that one should not *a priori* assume too simple a diagonal form for $\boldsymbol{\gamma}(\tau)$ in GGP models of dynamo fields. Indeed, in both models g and h, the time-averaged estimate $\bar{\mathbf{K}}(\tau)$ of this matrix has been shown to contain many significant non-diagonal terms testifying for spherical, equatorial and axial symmetry breaking properties. In order to make the best of a statistical analysis of the palaeomagnetic data, one should thus acknowledge that: (i) the autocovariances (or variances) $\gamma(x_n^m, x_n^m, \tau)$ may also depend on x, n and m; and (ii) the cross-covariances $\gamma(x_n^m, x_{n'}^{m'}, \tau)$ can be non-zero, even at time $\tau = 0$ relevant to palaeomagnetism. Only point (i) above has yet been partially recognized by some authors (e.g. Kono & Tanaka 1995; Constable & Johnson 1999; Kono *et al.* 2000a; see Paper I for a full review) and point (ii) has been raised only once by Hulot & Gallet (1996). Taking both points into account would clearly be desirable. However, it would have one drawback: requesting that the palaeomagnetic data be inverted for a covariance matrix defined by many more parameters than if it were purely diagonal. Fortunately, this inconvenience can be kept to a minimum, thanks to the fact, we also found, that estimates $\bar{K}(x_n^m, x_{n'}^{m'}, \tau)$ of the $\gamma(x_n^m, x_{n'}^{m'}, \tau)$ tend to take significant values only when $|n - n'|$ remains small. This is because the τ_n^m decrease as n increases (Tables 1 and 3; Figs 2 and 11) and because two Gauss coefficients with very different correlation times can hardly correlate with each other. This property can then be used to decide which $\gamma(x_n^m, x_{n'}^{m'}, \tau)$ may *a priori* be set to zero in the matrix, if we happen to be able to estimate the τ_n^m. Hulot & Le Mouël (1994; see also Harrison & Huang 1990) and Hongre *et al.* (1998) showed that historical and archeomagnetic data could provide enough information for this to be possible. Also, it turns out that the timescales involved are in fact quite similar to those found here for models g and h (see also Christensen & Olson 2003). Thus, taking the relevant non-diagonal $\boldsymbol{\gamma}(\tau)$ terms into account by applying the rule

$$\gamma\left(x_n^m, x_{n'}^{m'}, \tau\right) = 0 \qquad \text{if} \quad \tau_n^m \ll \tau_{n'}^{m'} \qquad \text{or} \quad \tau_n^m \gg \tau_{n'}^{m'} \tag{16}$$

would then guarantee that $\boldsymbol{\gamma}(\tau)$ does not involve that many more parameters than if it were purely diagonal. Such an approach would then make it possible to also rely on estimates of the covariance matrix $\boldsymbol{\gamma}(\tau)$ and not only of the mean field $\boldsymbol{\mu}$ to further investigate the symmetry breaking properties of the palaeomagnetic field. In fact, if further size reduction of $\boldsymbol{\gamma}(\tau)$ would really need to be implemented, then the best option would probably be to further assume eq. (8d) [i.e. $\gamma(x_n^m, x_{n'}^{m'}, \tau) = 0$ if $m \neq m'$], which would acknowledge the fact we found that detection of axial symmetry breaking in estimates of those terms anyway proves elusive.

Our results also revealed much more embarrassing characteristics of the fields produced by models g and h: some non-stationarity that can affect the MF produced by a dynamo and distort the distribution of the Gauss coefficients to the point it no longer is Gaussian. Those results are consistent with those of McMillan *et al.* (2001) who relied on a very different way of analysing the data. Taking those issues into account in the context of a GGP approach is not a simple matter. As illustrated by our results, the nature of this non-stationarity can indeed significantly differ from one case to another.

As pointed out by Coe *et al.* (2000) in an earlier study of the same simulations, it however turns out that artificial intensity records predicted from the model g field at the surface of the Earth compare quite well with the actual relative intensity records of deep-sea sediment cores, such as the one published by Valet & Meynadier (1993). Those cores indeed reveal significant intensity fluctuations on the 10 000 yr timescale, much more comparable to the modulations identified in model g (Fig. 8) than to those found in model h (Coe *et al.* 2000 also pointed out that similar predictions from model h did not compare well). [Incidentally, model g is also the one model producing a dominantly dipole family field (recall Table 2 and Fig. 3), a feature known to help produce a trend in the virtual geomagnetic pole (VGP) scatter curve similar to that observed for the past 5 Myr (Kono & Tanaka 1995; Hulot & Gallet 1996; Tauxe & Kent 2004), although in the present instance, the trend produced does not appear to be strong enough to explain the data (Glatzmaier *et al.* 1999).] We saw that the main cause of the departure from a Gaussian distribution was non-stationarity and that the not-so-severe non-stationarity seen in model g did not seriously affect the distribution of the Gauss coefficients. Those remained near-gaussian. The comparable amount of non-stationarity seen in both model g and the sediment cores thus suggests that a GGP approach could also safely be used to analyse at least the recent palaeomagnetic data.

Finally, it is worth commenting the intriguing difference found between models g and h, namely, the existence of two independent long-term modulations in model g as opposed to a single more complex modulation in model h. This difference somewhat mirrors the one found in the estimate $\bar{\mathbf{K}}(\tau)$ of the correlation matrix $\boldsymbol{\gamma}(\tau)$, revealing less correlations between the dipole and quadrupole families in model g than in model h. We noted that this meant that the fluctuating component of the model g field is statistically more symmetric with respect to the equator than that of model h. Unfortunately, no analogous statistical reasoning can be used to interpret the differences in the non-stationary modulations of models g and h. However, a very useful complementary deterministic approach can be invoked. It is indeed well known from kinematic dynamo theory that, if a dynamo flow is symmetric with respect to the equator, the two dipole and quadrupole family fields it generates become separable (i.e. are governed by two separate equations, Gubbins & Zhang 1993). Those fields may then behave independently, in very much the way they do in the case of model g [from the point of view of both the relative lack of correlation between the two families in $\bar{\mathbf{K}}(\tau)$ and the existence of independent modulations]. Indeed, we checked that, on average, the dynamo flow is more symmetric with respect to the equator in model g than in model h, though even in the case of model g, the flow is not found to be exactly symmetric. However, this observation also is not a surprise. A not-exactly-symmetric flow is indeed required to explain the weak but significant correlations found between the two families in model g[$\bar{\mathbf{K}}(\tau)$ is almost, but not exactly, compatible with eq. 9b/10b]. Furthermore, because model g is the result of a fully dynamic and not simply kinematic simulation, Lorentz forces associated with the field produced by the dynamo are bound to influence the flow. As a consequence, the flow may not remain symmetric with respect to the equator if the field produced is a mixture of the dipole and quadrupole family components (e.g. Gubbins & Zhang 1993). In the case of model g however, both the mean and fluctuating components of the field are dominated by terms from the dipole family and only a weak quadrupole family component is to be found (Table 2; Fig. 3). This is how both the non-symmetric flow and the coupling between the two family fields can remain weak, allowing model g to enjoy a dual modulation and weak correlations between the two families. By contrast, model h displays families of comparable magnitude (except of course for $\bar{g}_1^0$), especially in $\bar{\mathbf{K}}(\tau)$ (Table 4; Fig. 14), and enjoys both a single modulation and stronger correlations. In short, although from a purely statistical point of view, equatorial symmetry only requires that the mean field $\boldsymbol{\mu}$ belongs to either the dipole or quadrupole family, while the fluctuating field can be a mixture of both families (provided they display no cross-correlations, i.e. conform to eq. 9b/10b), dynamical considerations show that as soon as both families contribute similarly, especially to the fluctuating field, coupling between the two families will arise and so will correlations in $\boldsymbol{\gamma}(\tau)$.

6 CONCLUSION

In the present study, we addressed the pertinence of a GGP approach to characterize the statistical behaviour of fields produced by numerical simulations of dynamos. Those dynamos belong to the same general class of dynamos as the geodynamo producing the MF of the Earth. It may thus be argued that the conclusions reached here also likely pertain to the possibility of using a GGP approach to analyse the palaeomagnetic data and characterize the past behaviour of the geodynamo.

To be valid, the GGP approach requires that the Gauss coefficients define a vector $\mathbf{x}(t)$ behaving as the result of a multidimensional stationary Gaussian process with a short-term memory. Both models we investigated were found to enjoy a short-term memory. Some non-stationary behaviour was unfortunately found in both cases, causing some non-Gaussian behaviour, all the stronger that the non-stationarity was important. However, non-stationarity did not appear to be too serious of a problem if, as in model g, it remains within reasonable bounds, and occurs on timescales long compared to the memory of the process and short compared to the duration of a period of stable polarity. This seems to be the case for the real geodynamo, suggesting that a GGP approach can indeed be used to analyse the recent palaeomagnetic data.

However, estimating the mean field $\boldsymbol{\mu}$ and the covariance matrix $\boldsymbol{\gamma}(\tau)$ along the lines pioneered by Constable & Parker (1988) is not as simple a matter as one could wish, especially when one deals with (non-linear) directional data, in which case, as noted by Khokhlov *et al.* (2001), both $\boldsymbol{\mu}$ and $\boldsymbol{\gamma}(\tau)$ need to be estimated simultaneously. Because of that difficulty, all GGP modelling attempts made so far have relied on some additional assumptions with respect to the form $\boldsymbol{\gamma}(\tau)$ may take. In particular, $\boldsymbol{\gamma}(\tau)$ has always been assumed diagonal.

However, significant off-diagonal terms in the estimate $\bar{\mathbf{K}}(\tau)$ of $\boldsymbol{\gamma}(\tau)$ (cross-covariances) have been found in both models g and h, and are to be found for all rotating dynamos, as all of them break the spherical symmetry. Even under the most symmetric conditions (axial and equatorial), cross-covariances are found between Gauss coefficients sharing the same order and belonging to the same dipole/quadrupole family. Additional cross-covariances reaching across the two dipole/quadrupole families are otherwise found if equatorial symmetry is lost and even more cross-covariances may be found if, in addition, axial symmetry is lost as in model h. Similar off-diagonal terms in $\boldsymbol{\gamma}(\tau)$ must therefore exist in the case of the geodynamo. To make it possible to detect important symmetry breaking properties not only in $\boldsymbol{\mu}$ but also in $\boldsymbol{\gamma}(\tau)$, only the simple rule (16) based on timescales may safely be used to *a priori* decide which cross-covariances should be discarded.

As a matter of fact, the one symmetry breaking that appeared to be the easiest to detect, is equatorial symmetry breaking. However, it is found in both model h and the homogeneous model g. This

shows that, unfortunately, evidence of equatorial symmetry breaking possibly found in $\boldsymbol{\mu}$ and $\boldsymbol{\gamma}(\tau)$ [and in particular a $\mu(g_2^0)$ such as the one needed to explain the palaeomagnetic data], cannot as such be taken as evidence of equatorial symmetry breaking in the CMB conditions imposed on the dynamo. That is, unless, as pointed out in Paper I, the double case can be made that, every time the field reverses, both its dipole and quadrupole family components reverse simultaneously, while in the case of dynamos with equatorial symmetric CMB conditions, each family could reverse independently. Of course, we noted that stronger signatures for equatorial symmetry breaking are found in model h than in model g, suggesting that symmetry breaking CMB conditions could enhance the equatorial symmetry breaking properties of the field produced. However, we also noted that this enhancement is likely related to the fact that, contrary to that of model g, the fluctuating field of model h is not dominated by the dipole family. For dynamical reasons, this is bound to lead to stronger interactions between the two families. However, it is not unlikely that another dynamo regime running under equatorial symmetric CMB conditions could also be found, spontaneously breaking the equatorial symmetry like model g, and involving just as much quadrupole family and dipole family fluctuating fields as model h. This would then introduce more interactions between the two families, just as in model h.

Only axial symmetry breaking properties in $\boldsymbol{\mu}$ and $\boldsymbol{\gamma}(\tau)$ can in fact unambiguously testify for the influence of inhomogeneous CMB conditions. Such properties were found for model h (and not for model g). This shows that a similar influence could potentially be detected in the case of the real Earth. In $\boldsymbol{\gamma}(\tau)$, this would involve detecting either non-zero cross-covariances contradicting eq. (8d), or violations of equalities between autocovariances (8b) or non-zero cross-covariances (8c). However, violations of eq. (8d) proves elusive to detect. From a practical point of view, ignoring the possibility of such violations, i.e. assuming eq. (8d) holds [which conveniently reduces the number of terms involved in $\boldsymbol{\gamma}(\tau)$], and just checking for violations of eq. (8b-c), would probably be the most efficient way of investigating $\boldsymbol{\gamma}(\tau)$ for possible influence of inhomogeneous CMB conditions. In $\boldsymbol{\mu}$, the signature to be looked for is simpler (non-zonal terms), more easily detected and likely to at least partly reflect the inhomogoneous CMB conditions responsible for it (see also, Olson & Christensen 2002). However, it turns out that non-zonal terms in estimates of $\boldsymbol{\mu}$ remain quite weak. This, we noted, could be the reason why detection of non-zonal terms in the mean field derived from palaeomagnetic data still remains controversial. Our results suggest that additional data combined with a more appropriate treatment and analysis of the covariance matrix $\boldsymbol{\gamma}(\tau)$ could help settle the issue.

ACKNOWLEDGMENTS

We thank Cathy Constable and an anonymous reviewer for their constructive comments, which substantially helped improve the original manuscript. This research was completed while GH held a National Research Council Research Associateship Award at NASA Goddard Space Flight Center. Model g and model h geodynamo simulations were run at the Pittsburgh Supercomputing Center. Institut de Physique du Globe de Paris Contribution no. 2040 and Institut National des Sciences de l'univers (Centre National de la Recherche Scientifique) Contribution no. 378.

REFERENCES

Bloxham, J., 2000a. Core-mantle interactions and the palaeosecular variation, *Phil. Trans. R. Soc. Lond., A.,* **358,** 1171–1179.

Bloxham, J., 2000b. Sensitivity of the geomagnetic axial dipole to thermal core-mantle interactions, *Nature,* **405,** 63–65.

Carlut, J. & Courtillot, V., 1998. How complex is the time-averaged geomagnetic field over the past 5 Myr?, *Geophys. J. Int.,* **134,** 527–544.

Christensen, U.R. & Olson, P., 2003. Secular variation in numerical geodynamo models with lateral variations of boundary heat flow, *Phys. Earth planet. Int.,* **138,** 39–54.

Christensen, U., Olson, P. & Glatzmaier, G.A., 1998. A dynamo model interpretation of geomagnetic field structures, *Geophys. Res. Lett.,* **25,** 1565–1568.

Coe, R.S., Hongre, L. & Glatzmaier, G.A., 2000. An examination of simulated geomagnetic reversals from a palaeomagnetic perspective, *Phil. Trans. R. Soc. Lond., A.,* **358,** 1141–1170.

Constable, C.G. & Johnson, C.L., 1999. Anisotropic paleosecular variation models: implications for geomagnetic field observables, *Phys. Earth planet. Int.,* **115,** 35–51.

Constable, C.G. & Parker, R.L., 1988. Statistics of the geomagnetic secular variation for the past 5 m.y., *J. geophys. Res.,* **93,** 11 569–11 581.

Dormy, E., Valet, J.P. & Courtillot, V., 2000. Numerical models of the geodynamo and observational constraints, *Geochem. Geophys. Geosys.,* **1,** paper 2000GC000 062.

Glatzmaier, G.A. & Roberts, P.H., 1995. A three-dimensional convective dynamo solution with rotating and finitely conducting inner core and mantle, *Phys. Earth planet. Int.,* **91,** 63–75.

Glatzmaier, G.A. & Roberts, P.H., 1996. An anelastic evolutionary geodynamo simulation driven by compositional and thermal convection, *Physica D,* **97,** 81–94.

Glatzmaier, G.A. & Roberts, P.H., 1997. Simulating the geodynamo, *Contemp. Phys.,* **38,** 269–288.

Glatzmaier, G.A., Coe, R.S., Hongre, L. & Roberts, P.H., 1999. The role of the Earth's mantle in controlling the frequency of geomagnetic reversals, *Nature,* **401,** 885–890.

Gubbins, G. & Kelly, P., 1993. Persistent patterns in the geomagnetic field over the past 2.5 Myr, *Nature,* **365,** 829–832.

Gubbins, D. & Zhang, K., 1993. Symmetry properties of the dynamo equations for palaeomagnetism and geomagnetism, *Phys. Earth planet. Int.,* **75,** 225–241.

Harrison, C.G.A. & Huang, Q., 1990. Rates of change of the Earth's magnetic field measured by recent analyses, *J. Geomag. Geoelectr.,* **42,** 897–928.

Hongre, L., Hulot, G. & Khokhlov, A., 1998. An analysis of the geomagnetic field over the past 2000 years, *Phys. Earth planet. Int.,* **106,** 311–335.

Hulot, G. & Bouligand, C., 2005. Statistical paleomagnetic field modelling and symmetry considerations, *Geophys. J. Int.,* doi:10.1111/j.1365-246X.2005.02612 (this issue, Paper I).

Hulot, G. & Gallet, Y., 1996. On the interpretation of virtual geomagnetic pole (VGP) scatter curves, *Phys. Earth planet. Int.,* **95,** 37–53.

Hulot, G. & Le Mouël, J.L., 1994. A statistical approach to the Earth's main magnetic field., *Phys. Earth planet. Int.,* **82,** 167–183.

Hulot, G., Eymin, C., Langlais, B., Mandea, M. & Olsen, N., 2002. Small-scale structure of the geodynamo inferred from Oersted and Magsat satellite data, *Nature,* **416,** 620–623.

Johnson, C.L. & Constable, C.G., 1997. The time averaged geomagnetic field: global and regional biases for 0–5 Ma, *Geophys. J. Int.,* **131,** 643–666.

Khokhlov, A., Hulot, G. & Carlut, J., 2001. Towards a self-consistent approach to paleomagnetic field modeling, *Geophys. J. Int.,* **145,** 157–171.

Kono, M. & Roberts, P.H., 2002. Recent geodynamo simulations and observations of the geomagnetic field, *Rev. Geophys.,* **40**(4), 1013, 10.1029/2000RG000102.

Kono, M. & Tanaka, H., 1995. Mapping the Gauss coefficients to the pole and the models of paleosecular variation, *J. Geomag. Geoelectr.,* **47,** 115–130.

Kono, M., Tanaka, H. & Tsukanawa, H., 2000a. Spherical harmonic analysis of paleomagnetic data: the case of linear mapping, *J. geophys. Res.,* **105,** 5817–5833.

Kono, M., Sakuraba, A. & Ishida, M., 2000b. Dynamo simulations and paleosecular variation models., *Phil. Trans. R. Soc. Lond.,* A, **358,** 1123–1139.

Kuang, W. & Bloxham, J., 1997. An Earth-like numerical dynamo model, *Nature,* **389,** 371–374.

McElhinny, M.W., McFadden, P.L. & Merrill, R.T., 1996. The time-averaged paleomagnetic field 0–5 Ma, *J. geophys. Res.,* **101,** 25 007–25 027.

McMillan, D.G., Constable, C.G., Parker R.L. & Glatzmaier, G.A., 2001. A statistical analysis of magnetic fields from some geodynamo simulations, *Geochem. Geophys. Geosys.,* **2,** paper 2000GC000 130.

Merrill, R.T. & McFadden, P.L., 2003. The geomagnetic axial dipole field assumption, *Phys Earth planet. Int.,* **139,** 171–185.

Merrill, R.T., McElhinny, M.W. & McFadden, P.L., 1996. *The Magnetic Field of the Eaaleomagnetism, the Core, and the Deep Mantle,* Academic, San Diego, CA, p. 527.

Olson, P. & Christensen, U.R., 2002. The time-average magnetic field in numerical dynamos with non-uniform boundary heat flow, *Geophys. J. Int.,* **151,** 809–823.

Press, W.H., Teukolsky, S.A., Vetterling, W.T. & Flannery, B.P., 1992. *The art of Scientific Computing, Numerical Recipes in C,* Cambridge Univ. Press, Cambridge, p. 994.

Tauxe, L. & Kent, D., 2004. A simplified statistical model for the geomagnetic field and the detection of shallow bias in paleomagnetic inclinations: was the ancient magnetic field dipolar?, in *Timescales of the Paleomagnetic field* eds Channell J.E.T., Kent D.V., Lowrie W. & Meert J. *Am. geophys. Un. Monogr.,* **145,** 101–115.

Valet, J.P. & Meynadier, L., 1993. Geomagnetic field intensity and reversals during the past four million years, *Nature,* **366,** 234–238.

van der Waerden, B.L., 1969. *Mathematical statistics,* Springer-Verlag, New York, p. 367.